LETTER

doi:10.1038/nature22798

BAP1 regulates IP3R3–mediated Ca^{2+} flux to mitochondria suppressing cell transformation

Angela Bononi[1], Carlotta Giorgi[2], Simone Patergnani[2], David Larson[1], Kaitlyn Verbruggen[1], Mika Tanji[1], Laura Pellegrini[1], Valentina Signorato[1,2], Federica Olivetto[1,2], Sandra Pastorino[1], Masaki Nasu[1], Andrea Napolitano[1], Giovanni Gaudino[1], Paul Morris[1], Greg Sakamoto[1], Laura K. Ferris[3], Alberto Danese[2], Andrea Raimondi[4], Carlo Tacchetti[4,5], Shafi Kuchay[6], Harvey I. Pass[6], El Bachir Affar[7], Haining Yang[1], Paolo Pinton[2] & Michele Carbone[1]

BRCA1-associated protein 1 (*BAP1*) is a potent tumour suppressor gene that modulates environmental carcinogenesis[1–3]. All carriers of inherited heterozygous germline *BAP1*-inactivating mutations (*BAP1*$^{+/-}$) developed one and often several *BAP1*$^{-/-}$ malignancies in their lifetime[4], mostly malignant mesothelioma, uveal melanoma[2,5], and so on[6–10]. Moreover, *BAP1*-acquired biallelic mutations are frequent in human cancers[8,11–14]. BAP1 tumour suppressor activity has been attributed to its nuclear localization, where it helps to maintain genome integrity[15–17]. The possible activity of BAP1 in the cytoplasm is unknown. Cells with reduced levels of BAP1 exhibit chromosomal abnormalities and decreased DNA repair by homologous recombination[18], indicating that BAP1 dosage is critical. Cells with extensive DNA damage should die and not grow into malignancies. Here we discover that BAP1 localizes at the endoplasmic reticulum. Here, it binds, deubiquitylates, and stabilizes type 3 inositol-1,4,5-trisphosphate receptor (IP3R3), modulating calcium (Ca^{2+}) release from the endoplasmic reticulum into the cytosol and mitochondria, promoting apoptosis. Reduced levels of BAP1 in *BAP1*$^{+/-}$ carriers cause reduction both of IP3R3 levels and of Ca^{2+} flux, preventing *BAP1*$^{+/-}$ cells that accumulate DNA damage from executing apoptosis. A higher fraction of cells exposed to either ionizing or ultraviolet radiation, or to asbestos, survive genotoxic stress, resulting in a higher rate of cellular transformation. We propose that the high incidence of cancers in *BAP1*$^{+/-}$ carriers results from the combined reduced nuclear and cytoplasmic activities of BAP1. Our data provide a mechanistic rationale for the powerful ability of BAP1 to regulate gene–environment interaction in human carcinogenesis.

BAP1 is a member of the ubiquitin carboxy (C)-terminal hydrolase (UCH) subfamily of deubiquitylating enzymes[2]. The ubiquitin-conjugating enzyme UBE2O induces BAP1 sequestration in the cytoplasm by multi-monoubiquitylation of its nuclear localization signal (NLS). BAP1 counteracts this mechanism and regulates its own nuclear translocation by intra-molecular auto-deubiquitylation of the same sites[19]. Since there is a well-established mechanism to keep BAP1 in the cytoplasm, BAP1 may also exert some cytoplasmic activity. We tested this hypothesis in primary fibroblasts we derived from skin punch biopsies from members of the W and L families, in which we originally discovered that BAP1 mutations caused a novel cancer syndrome, the 'BAP1 cancer syndrome'[2,5].

About 50% of the W and L family members inherited *BAP1* mutations[2,5]. We established fibroblast cell cultures from seven *BAP1*$^{+/-}$ carriers and from seven age- and gender-matched wild-type *BAP1* (*BAP1*^{WT}) control family members (Supplementary Fig. 1a, b). Therefore, one of the main strengths of our data is that they are specific to the human condition and cannot be influenced by factors other than the reduced levels of BAP1, such as, for example, the many genetic mutations that are found in all tumour-derived cell lines. Cells from *BAP1*$^{+/-}$ carriers contained approximately 50% of BAP1 protein compared with controls (Extended Data Fig. 1a–d) and did not show any differences in growth or cell cycle progression (Extended Data Fig. 1e, f).

Annexin V and propidium iodide staining, and western blot measuring cleaved caspase-3 levels, revealed that seven out of seven *BAP1*$^{+/-}$ fibroblast cell cultures were more resistant to various apoptotic drugs than seven matched *BAP1*^{WT} fibroblast cell cultures (Fig. 1a, b and Extended Data Fig. 1g–l). We obtained similar results by downregulating BAP1 in *BAP1*^{WT} primary human mesothelial cells (Extended Data Fig. 1m).

Although all known activities of BAP1 have been ascribed to its nuclear localization[2], apoptosis is a process largely regulated in the cytoplasm. Subcellular fractionation of primary *BAP1*^{WT} fibroblasts, human mesothelial cells, cells of the malignant mesothelioma cell lines PPM-Mill, and HEK293 (Extended Data Fig. 2a) revealed that extra-nuclear BAP1 was specifically present in the endoplasmic reticulum (ER) fraction, findings confirmed by electron microscopy (Fig. 1c) and immunofluorescence (Extended Data Fig. 2b–e). BAP1 ER levels were reduced more than nuclear levels in *BAP1*$^{+/-}$ fibroblasts (Fig. 1d and Extended Data Fig. 2f–h).

The ER is the major store of intracellular Ca^{2+} (refs 20, 21). IP3Rs are ER channels that control Ca^{2+} release from the ER to the cytoplasm and the mitochondria[22,23]. Transient Ca^{2+} release promotes mitochondrial ATP production; excessive or prolonged Ca^{2+} release triggers apoptosis via mitochondrial Ca^{2+} overload and opening of the mitochondrial permeability transition pore[24]. The drugs shown in Fig. 1a, b and Extended Data Fig. 1g–m induce apoptosis via ER Ca^{2+} release[25]. We hypothesized that BAP1 was involved in the regulation of intracellular Ca^{2+} homeostasis. We transfected *BAP1*$^{+/-}$ and *BAP1*^{WT} fibroblasts with ER-targeted cameleon (D1ER), a fluorescent probe to measure Ca^{2+} concentrations[23]. Cells were stimulated with bradykinin, an agonist that causes ER Ca^{2+} release through the IP3Rs, or with H_2O_2. Compared with *BAP1*^{WT}, *BAP1*$^{+/-}$ fibroblasts released lower amounts of Ca^{2+} from the ER (Fig. 1e, Extended Data Fig. 3a–c and Supplementary Table 1), findings suggestive of reduced flow of Ca^{2+} through the IP3Rs. Accordingly, we detected lower Ca^{2+} concentrations in the cytosol and the mitochondrial matrix of *BAP1*$^{+/-}$ compared with *BAP1*^{WT} fibroblasts stimulated with bradykinin (Fig. 1f, Extended Data Fig. 3d–g and Supplementary Tables 1 and 2) or H_2O_2 (Extended Data Fig. 3h–m and Supplementary Tables 1 and 2), independently of extracellular Ca^{2+} influx from the plasma membrane (Extended Data Fig. 3n and Supplementary Table 1). The results were reproducible in all seven *BAP1*$^{+/-}$ and seven matching *BAP1*^{WT} fibroblasts studied, as well as in three cell cultures of primary human mesothelial cells in which *BAP1*

[1]University of Hawaii Cancer Center, University of Hawaii, Honolulu, Hawaii 96813 USA. [2]Department of Morphology, Surgery and Experimental Medicine, University of Ferrara, Ferrara, 44121 Italy. [3]Department of Dermatology, University of Pittsburgh Medical Center, Pittsburgh, Pennsylvania, 15213 USA. [4]Experimental Imaging Center, San Raffaele Scientific Institute Milano, 20132 Italy. [5]Department of Experimental Medicine, University of Genova, Genova, 16132 Italy. [6]Cancer Center, New York University, New York, New York 10016, USA. [7]Maisonneuve-Rosemont Hospital Research Center, Department of Medicine, University of Montréal, Montréal, Quebec H1T 2M4, Canada.

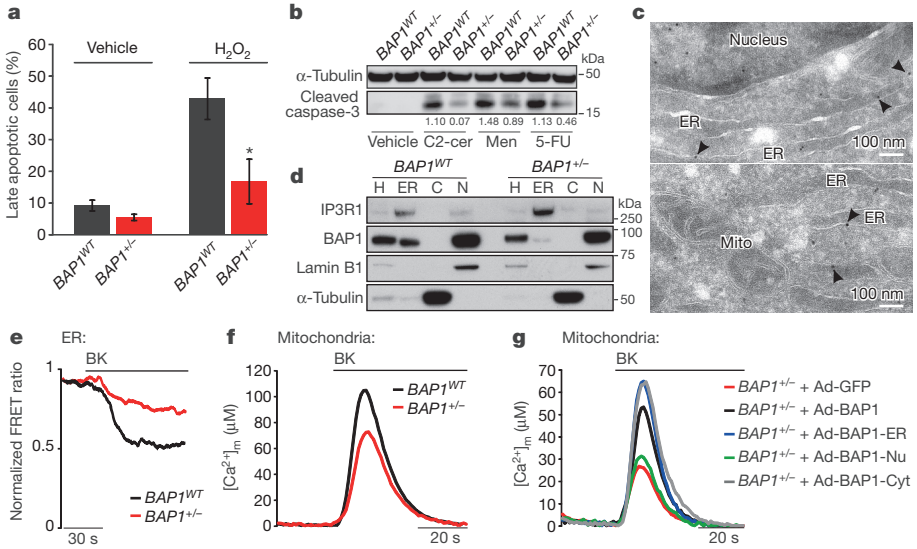

Figure 1 | BAP1 localizes at the ER and modulates Ca^{2+} signalling and apoptosis. a, **b**, Reduced apoptosis in *BAP1*$^{+/-}$ L-fibroblasts treated with 100 μM H_2O_2 (**a**) or with 10 μM C2-ceramide (C2-cer), 10 μM menadione (Men) or 10 μM 5-fluorouracil (5-FU) (**b**). Decimals: cleaved caspase-3/α-tubulin. **a**, Data shown as mean ± s.e.m. of $n = 4$ independent experiments (three biological replicates, one culture replicate) with pooled analysis displayed. *P* value calculated using two-tailed unpaired Student's *t*-test, $*P < 0.05$. **c**, **d**, BAP1 localizes at the ER. **c**, Electron microscopy, immunogold labelling of *BAP1*^{WT} fibroblasts; arrowheads, ER-localized BAP1. Mito, mitochondria; scale bar, 100 nm. **d**, Subcellular fractionation: ER BAP1 levels. H, homogenate; C, cytosol; N, nuclei. Markers: ER (IP3R1), nuclei (Lamin B1), cytosol (α-tubulin). **e**, **f**, *BAP1*$^{+/-}$ L-fibroblasts stimulated with 1 μM bradykinin (BK) show reduced ER Ca^{2+} release (**e**) and mitochondrial Ca^{2+} concentrations ($[Ca^{2+}]_m$) (**f**). **g**, Cytoplasmic- and ER-targeted BAP1 (Ad-BAP1-Cyt and Ad-BAP1-ER) restore $[Ca^{2+}]_m$ to levels similar or higher than *BAP1*$^{+/-}$ fibroblasts transduced with BAP1 (Ad-BAP1), nuclear BAP1 (Ad-BAP1-Nu) does not. **e**–**g**, For source data, see Supplementary Tables 1 and 2. For western blot and electron microscopy source images, see Supplementary Figs 2 and 3.

was silenced (Extended Data Fig. 3o, p and Supplementary Table 2). We obtained similar results in mice adult fibroblasts (MAFs) we derived from *Bap1*$^{+/-}$ mice[3] compared with *Bap1*^{WT} mice (Extended Data Fig. 3q, r and Supplementary Table 2).

To test whether cytoplasmic BAP1 modulates Ca^{2+} fluxes independently from nuclear BAP1, we built three adenoviral chimaeras that specifically localized BAP1 to the nucleus (BAP1-Nu), the cytoplasm (BAP1-Cyt), and the outer surface of the ER (BAP1-ER) (Extended Data Fig. 4a): only the cytoplasmic and ER chimaeras regulated Ca^{2+} changes (Fig. 1g, Extended Data Fig. 4b and Supplementary Tables 1 and 2).

IP3Rs can be rapidly ubiquitylated and degraded by the proteasome[26]. Fibroblasts from *BAP1*$^{+/-}$ donors contained reduced IP3R3 protein levels (the isoform that controls apoptosis[27]) compared with *BAP1*^{WT} (Fig. 2A, B and Extended Data Fig. 5a–c). Similarly, human malignant mesothelioma cells with mutated *BAP1* (>60% of sporadic malignant mesotheliomas carry somatic *BAP1* mutations[11,14]) contained reduced levels of IP3R3 (Extended Data Fig. 5d). IP3R3 messenger RNA (mRNA) (*ITPR3*) levels measured by quantitative PCR with reverse transcription (qRT–PCR) were similar in *BAP1*^{WT} and *BAP1*$^{+/-}$ fibroblasts (Extended Data Fig. 5e), suggesting that the differences observed were not transcriptionally regulated. We hypothesized that BAP1 might deubiquitylate and stabilize IP3R3. We found that IP3R3 co-immunoprecipitated BAP1 (Fig. 2C), findings supported by proximity ligation assay (Fig. 2D) and immunofluorescence (Extended Data Fig. 6a). BAP1–IP3R3 co-immunoprecipitate was barely detectable in *BAP1*$^{+/-}$ fibroblasts; BAP1 rescue significantly increased the amount of BAP1 that co-immunoprecipitated with IP3R3 (Fig. 2E). We confirmed the specificity of the BAP1 interaction with IP3R3 in HEK293 cells expressing Flag–BAP1 (Extended Data Fig. 6b). Instead, overexpression of the Myc-tagged truncated BAP1 L-mutant (Myc–BAP1(L)) (the L family mutant BAP1, which lacks the amino (N) terminus domain[5]) showed an almost complete loss of interaction with IP3R3 compared with Myc-tagged wild-type BAP1 (Myc–BAP1) (Fig. 2F), while catalytically inactive BAP1(C91S)[2,19] did bind IP3R3 (Extended Data Fig. 6c). We found that BAP1 binds the N terminus domain of IP3R3 (IP3R3(NT)) (Fig. 2G). Deletion fragments of BAP1 revealed that its catalytic domain (UCH) did not bind IP3R3(NT), while its middle portion (NORS) and, to a minor extent, the C-terminal portion (CTD, NLS) did (Extended Data Fig. 6e, f). Overexpression of the N terminus of the IP3R3 bound and sequestered BAP1, leading to decreased IP3R3 levels, an effect counterbalanced by BAP1 co-overexpression (Extended Data Fig. 6d).

Silencing of BAP1 in *BAP1*^{WT} fibroblasts consistently caused a reduction of IP3R3 protein levels (Extended Data Fig. 7a), with a concomitant reduction in mitochondrial Ca^{2+} responses (Extended Data Fig. 7b, c and Supplementary Tables 1 and 2), and protection from apoptosis (Extended Data Fig. 7d). Likewise, silencing of IP3R3 (Extended Data Fig. 7e) in *BAP1*^{WT} fibroblasts reduced mitochondrial Ca^{2+} concentration (Extended Data Fig. 7f, g and Supplementary Tables 1 and 2) and apoptosis (Extended Data Fig. 7h). Similar results were obtained in human mesothelial cells (Extended Data Fig. 7i, j and Supplementary Table 2). Transduction of *BAP1*$^{+/-}$ fibroblasts with adenoviruses encoding BAP1, but not the catalytically inactive mutant BAP1(C91S)[2,19], rescued IP3R3 protein levels (Fig. 3a) and mitochondrial Ca^{2+} uptake (Fig. 3b, Extended Data Fig. 8j and Supplementary Tables 1 and 2), and resulted in enhanced apoptosis (Fig. 3c). Similar results were obtained in Phi and HMESO cells (derived from two human malignant mesotheliomas with biallelic BAP1 mutations) in which we reintroduced BAP1 or BAP1(C91S), and in human mesothelial cells in which we silenced BAP1 and then reintroduced BAP1 or BAP1(C91S). BAP1 stabilized IP3R3 and increased mitochondrial Ca^{2+} concentrations and apoptosis; BAP1(C91S) did not (Extended Data Fig. 8a–h and Supplementary Table 2). Moreover, in contrast to BAP1, mutated BAP1(W) and BAP1(L) did not influence mitochondrial calcium concentration ($[Ca^{2+}]_m$) after 1 μM bradykinin stimulation (Extended Data Fig. 8i and Supplementary Table 2).

In vitro ubiquitylation assays using purified recombinant proteins revealed that BAP1 counteracted the ubiquitylation of IP3R3(NT)

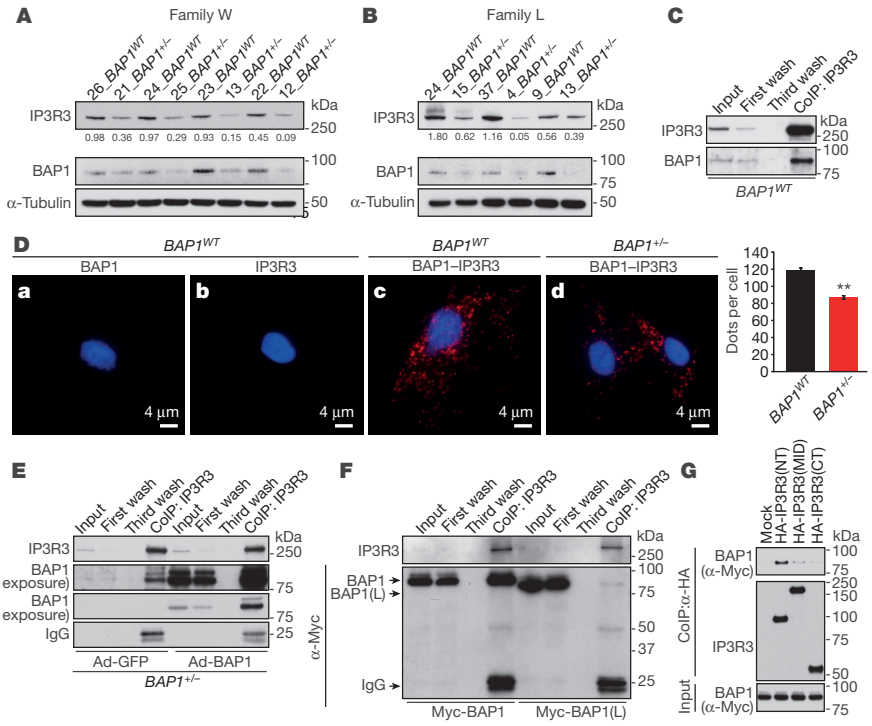

Figure 2 | IP3R3 and BAP1 interaction. **A**, **B**, Western blot, reduced IP3R3 levels in *BAP1*$^{+/-}$ fibroblasts. Decimals: IP3R3/α-tubulin. **C**–**G**, BAP1–IP3R3 interaction. **C**, Co-immunoprecipitation (CoIP) of IP3R3–BAP1, *BAP1*^{WT} fibroblasts. **D**, Proximity ligation assay; red dots show IP3R3–BAP1 interaction in *BAP1*^{WT} (**c**) and *BAP1*$^{+/-}$ (**d**) fibroblasts; **a**, **b**, controls using only one antibody. Nuclei stained blue with 4′,6-diamidino-2-phenylindole (DAPI). Scale bar, 4 μm. Bar graph: quantification of proximity ligation assay red dots per cell showing reduced IP3R3–BAP1 interaction in *BAP1*$^{+/-}$ fibroblasts. Data shown as mean ± s.e.m. ($n = 11$ cells per condition). *P* value calculated using two-tailed unpaired Student's *t*-test, $^{**}P < 0.01$. **E**, Co-immunoprecipitation of IP3R3–BAP1 in *BAP1*$^{+/-}$ fibroblasts transduced with adenovirus GFP (Ad-GFP) or Ad-BAP1. **F**, Co-immunoprecipitation of IP3R3–BAP1 in HEK293 transfected with Myc-tagged wild-type BAP1; note reduced co-immunoprecipitate with truncated BAP1(L). **G**, BAP1 binds the IP3R3 N terminus. Co-immunoprecipitation of IP3R3–BAP1 in HEK293 co-transfected with Myc-tagged BAP1 and haemagglutinin (HA)-tagged IP3R3 deletion mutants ((NT, amino acids 1–800), (MID, amino acids 801–2230), (CT, amino acids 2180–2670). First and third wash lanes show progressive loss of bound proteins during sequential washes confirming specificity of co-immunoprecipitation. For western blot source images, see Supplementary Fig. 2.

(Fig. 3d). The *in vitro* deubiquitylating activity of BAP1 on IP3R3(NT) became detectable 30 min after adding BAP1 to the reaction, and was stronger at 60 min (Fig. 3e). BAP1(C91S), despite being able to bind IP3R3 (Extended Data Fig. 6c), failed to deubiquitylate IP3R3(NT) (Fig. 3d, e and Extended Data Fig. 8k, l), emphasizing the requirement of BAP1 catalytic activity.

Comet assays showed that *BAP1*$^{+/-}$ fibroblasts had a reduced ability to repair DNA damage after exposure to ionizing radiation (Fig. 4a and Extended Data Fig. 9a), findings supported by kinetics analyses showing a prolonged phosphorylation of γ-H2A.X indicating that DNA repair was delayed (Fig. 4b). Despite the reduced ability of *BAP1*$^{+/-}$ cells to repair ionizing radiation-induced DNA damage, clonogenic assays revealed increased survival of *BAP1*$^{+/-}$ cells compared with *BAP1*^{WT} after ionizing radiation (Fig. 4c and Extended Data Fig. 9b). Moreover, ultraviolet radiation with UVA (340 nm) or UVB (312 nm) (UVB is a more potent carcinogen than UVA) induced ER Ca^{2+} release, which was significantly impaired in *BAP1*$^{+/-}$ fibroblasts (Extended Data Fig. 9c–e), and UVB induced prolonged phosphorylation of γ-H2A.X (Extended Data Fig. 9f). Clonogenic assays in fibroblasts from *BAP1*$^{+/-}$ individuals and matched controls, exposed to UVA or

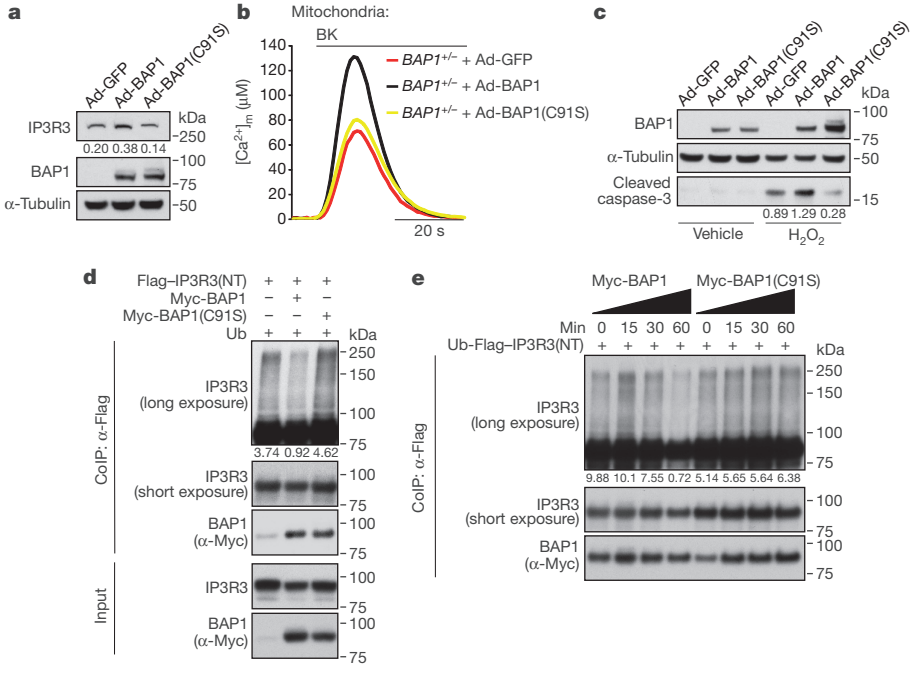

Figure 3 | BAP1 deubiquitylates IP3R3. **a**–**c**, Wild-type BAP1, not catalytically inactive BAP1(C91S), stabilizes IP3R3 (**a**), increases $[Ca^{2+}]_m$ after 1 μM bradykinin stimulation (**b**), and enhances apoptosis (**c**). Decimals: IP3R3 or cleaved caspase-3/α-tubulin. **d**, Ubiquitylation assay: wild-type BAP1, not BAP1(C91S), deubiquitylates the IP3R3 N terminus. HEK293 co-transfected with Flag–IP3R3(NT) and either Myc–BAP1, Myc–BAP1(C91S) or empty vector. Ub, Ubiquitin. **e**, Ubiquitylation/deubiquitylation assay. Immunopurified Myc–BAP1 or catalytically inactive Myc–BAP1(C91S) was incubated *in vitro* with ubiquitylated Flag–IP3R3(NT), followed by western blot. The ladder corresponds to ubiquitylated IP3R3(NT). Decimals: ubiquitylated IP3R3(NT) normalized to total immunoprecipitated IP3R3(NT) at 90 kDa (short exposure). For western blot source images, see Supplementary Fig. 2. **b**, For source data, see Supplementary Table 2.

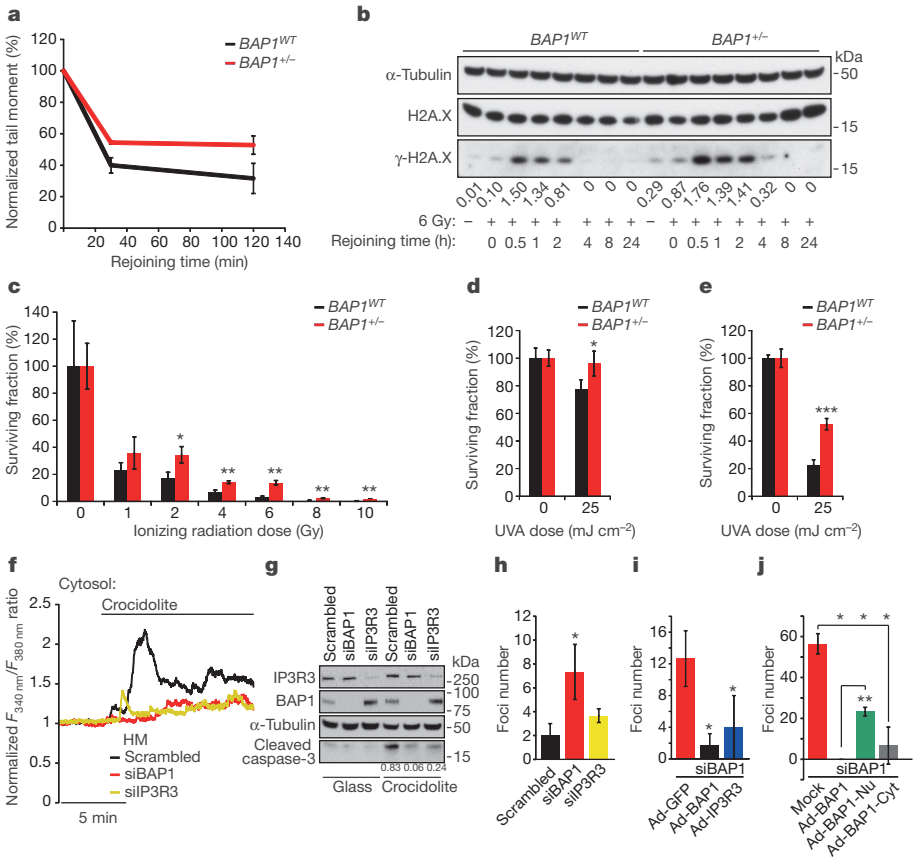

Figure 4 | Reduced nuclear and cytoplasmic BAP1 levels increase survival from DNA damage, resistance to apoptosis, and foci formation. **a**–**c**, Reduced (**a**, comet assay), delayed (**b**, γ-H2A.X kinetics) DNA repair, and increased survival (**c**, clonogenic assays) in *BAP1*$^{+/-}$ fibroblasts after ionizing radiation. Decimals: γ-H2A.X/H2A.X. **a**, $N = 2$ biological replicates with pooled analysis displayed, representative of three independent experiments. **a**, **c**, See Extended Data Fig. 9a, b. **b**, For western blot source images, see Supplementary Fig. 2. **d**, **e**, Clonogenic assays: increased survival of *BAP1*$^{+/-}$ fibroblasts after 25 mJ cm^{-2} UVA (**d**) or UVB (**e**) radiation; see Extended Data Fig. 9g. **f**, ER Ca^{2+} release in primary human mesothelial cells (HM) exposed to asbestos and transfected with siBAP1 or siIP3R3, or scrambled (see Extended Data Fig. 10a); for source data, see Supplementary Table 1. **g**, Reduced apoptosis in human mesothelial cells silenced for either BAP1 or IP3R3 exposed to asbestos. Western blot comparing cleaved caspase-3 levels (see Extended Data Fig. 10b). Decimals: cleaved caspase-3/α-tubulin. **h**–**j**, Cytoplasmic BAP1 and IP3R3 levels influence foci formation in human mesothelial cells exposed to asbestos. Foci formation in human mesothelial cells silenced with scrambled siRNA, siBAP1, and siIP3R3 (**h**); human mesothelial cells silenced for BAP1 and transduced with Ad-GFP (control), Ad-BAP1, and Ad-IP3R3 (**i**); and human mesothelial cells silenced for BAP1 and transduced with Ad-BAP1, Ad-BAP1-Nu, and Ad-BAP1-Cyt (**j**). **c**–**e**, **h**–**j**, $N = 3$ culture replicates, representative of three (**c**, **e**, **h**, **i**) or two (**d**, **j**) independent experiments in biological replicates. Data shown as mean ± s.d. *P* value calculated using two-tailed unpaired Student's *t*-tests. $*P < 0.05$; $**P < 0.01$; $***P < 0.001$.

UVB, revealed a reproducible significant increase in colony formation in *BAP1*$^{+/-}$ fibroblasts (24% increase with UVA, 132% with UVB) (Fig. 4d, e and Extended Data Fig. 9g).

Moreover, we discovered that crocidolite asbestos increased intracellular Ca^{2+} concentrations (Fig. 4f, Extended Data Fig. 10a and Supplementary Table 1) and apoptosis (Fig. 4g and Extended Data Fig. 10b). Human mesothelial cells silenced for either BAP1 or IP3R3 and exposed to crocidolite displayed reduced intracellular Ca^{2+} concentrations (Fig. 4f, Extended Data Fig. 10a and Supplementary Table 1) and were resistant to apoptosis (Fig. 4g and Extended Data Fig. 10b). Similar results were obtained in THP-1, a human monocytic cell line in which we downregulated BAP1 with short interfering RNA (siRNA), emphasizing the general relevance of this mechanism (Extended Data Fig. 10c–e and Supplementary Table 2). We used an established protocol in which primary human mesothelial cells exposed to crocidolite in the presence of tumour necrosis factor-alpha (TNFα) underwent *in vitro* transformation, measured as formation of three-dimensional foci[28]. Human mesothelial cells treated with siBAP1 and exposed to crocidolite showed a significant increase in foci formation (Fig. 4h). Silencing of IP3R3 was less effective in increasing foci formation than BAP1 silencing, indicating that both nuclear and cytoplasmic BAP1 act in concert to prevent malignant transformation (Fig. 4h). Moreover, transduction of either BAP1 or IP3R3 in human mesothelial cells silenced for BAP1 significantly reduced foci formation (Fig. 4i). To test the independent contribution of cytoplasmic and nuclear BAP1 to cellular transformation, we silenced BAP1 and then infected human mesothelial cells with the BAP1 chimaeras (Extended Data Fig. 4a). Transduction with BAP1-Cyt that specifically localized to the cytoplasm, where it modulated intracellular Ca^{2+} fluxes (Fig. 1g), significantly reduced foci formation to levels similar to those obtained using BAP1 (Fig. 4j). Cells infected with BAP1-Nu, which localized only to the nucleus, showed reduced foci formation although the reduction was significantly less than cells infected with BAP1 (Fig. 4j).

It is unlikely that mutated cytoplasmic BAP1 contributed to some of the biological effects observed. With one single exception in one case of uveal melanoma[12], all BAP1 mutations described impair the ability of BAP1 to translocate into the nucleus, either because the NLS is deleted, as in the L and W *BAP1*$^{+/-}$ fibroblasts studied here, or because the catalytic domain is inactive[8,11–14,19]. Mutated cytoplasmic BAP1 forms amyloid-like aggregates and is biologically inactive[29], although it may be detectable by immunostaining[2,5,11]. In the W and L cells, truncation removed a critical domain for the interaction with IP3R3 (Fig. 2F). Accordingly, mutated W and L BAP1 did not influence Ca^{2+} signalling (Extended Data Fig. 8i and Supplementary Table 2).

In summary, we have discovered that in the cytoplasm BAP1 localizes at the ER, where it binds, deubiquitylates, and stabilizes IP3R3, thus regulating ER Ca^{2+} release and promoting apoptosis. Decreased levels of BAP1 lead to enhanced DNA damage (because of decreased nuclear BAP1 activity), reduced apoptosis (because of decreased cytoplasmic BAP1 activity), and increased cellular transformation (because of both decreased nuclear and cytoplasmic activities). The separate activities of BAP1 in the nucleus and cytoplasm provide a mechanistic rationale for the strong tumour suppressor activity of this deubiquitylase. Our data suggest that the reduced levels of BAP1 result in a tumour phenotype prevalently under genotoxic/stress conditions (gene–environment interaction). Accordingly, 70% of *BAP1*$^{+/-}$ heterozygous mice developed malignant mesotheliomas within a year when exposed to asbestos, and none of the non-exposed *BAP1*$^{+/-}$ mice developed malignant mesotheliomas during the same period[3]. Although almost any tumour type has been reported in carriers of germline *BAP1* mutations[1,2,4–10], there is a prevalence of malignant mesothelioma, often caused by asbestos, and of melanomas and skin cancers, often caused by ultraviolet radiation[4]. These two environmental carcinogens induce DNA damage and cell death. The balance between DNA damage and cell death determines the outcome: the more DNA-damaged cells survive exposure, the higher the risk that one of them may grow into a malignancy. It is possible that the malignancies more frequently associated with the BAP1 cancer syndrome arise from tissues in which Ca^{2+}-induced apoptosis plays a critical role in cellular transformation.

Our findings reveal the relevance of post-translational modifications in modulating gene–environment interactions in human carcinogenesis, are relevant to understanding the high incidence of environmentally related cancers in carriers of germline *BAP1* mutations, and provide novel targets for the numerous human malignancies that carry acquired and inherited *BAP1* mutations[1,2,6–13,30].

Online Content Methods, along with any additional Extended Data display items and Source Data, are available in the online version of the paper; references unique to these sections appear only in the online paper.

Received 3 August 2016; accepted 28 April 2017.
Published online 14 June 2017.

1. Carbone, M. *et al.* Consensus Report of the 2015 Weinman International Conference on Mesothelioma. *J. Thorac. Oncol.* **11,** 1246–1262 (2016).
2. Carbone, M. *et al.* BAP1 and cancer. *Nat. Rev. Cancer* **13,** 153–159 (2013).
3. Napolitano, A. *et al.* Minimal asbestos exposure in germline BAP1 heterozygous mice is associated with deregulated inflammatory response and increased risk of mesothelioma. *Oncogene* **35,** 1996–2002 (2016).
4. Baumann, F. *et al.* Mesothelioma patients with germline BAP1 mutations have 7-fold improved long-term survival. *Carcinogenesis* **36,** 76–81 (2015).
5. Testa, J. R. *et al.* Germline BAP1 mutations predispose to malignant mesothelioma. *Nat. Genet.* **43,** 1022–1025 (2011).
6. de la Fouchardière, A. *et al.* Germline BAP1 mutations predispose also to multiple basal cell carcinomas. *Clin. Genet.* **88,** 273–277 (2015).
7. Njauw, C. N. *et al.* Germline BAP1 inactivation is preferentially associated with metastatic ocular melanoma and cutaneous-ocular melanoma families. *PLoS ONE* **7,** e35295 (2012).
8. Jiao, Y. *et al.* Exome sequencing identifies frequent inactivating mutations in BAP1, ARID1A and PBRM1 in intrahepatic cholangiocarcinomas. *Nat. Genet.* **45,** 1470–1473 (2013).
9. Farley, M. N. *et al.* A novel germline mutation in BAP1 predisposes to familial clear-cell renal cell carcinoma. *Mol. Cancer Res.* **11,** 1061–1071 (2013).
10. Abdel-Rahman, M. H. *et al.* Germline BAP1 mutation predisposes to uveal melanoma, lung adenocarcinoma, meningioma, and other cancers. *J. Med. Genet.* **48,** 856–859 (2011).
11. Nasu, M. *et al.* High incidence of somatic BAP1 alterations in sporadic malignant mesothelioma. *J. Thorac. Oncol.* **10,** 565–576 (2015).
12. Harbour, J. W. *et al.* Frequent mutation of BAP1 in metastasizing uveal melanomas. *Science* **330,** 1410–1413 (2010).
13. Peña-Llopis, S. *et al.* BAP1 loss defines a new class of renal cell carcinoma. *Nat. Genet.* **44,** 751–759 (2012).
14. Yoshikawa, Y. *et al.* High-density array-CGH with targeted NGS unmask multiple noncontiguous minute deletions on chromosome 3p21 in mesothelioma. *Proc. Natl Acad. Sci. USA* **113,** 13432–13437 (2016).
15. Lee, H. S., Lee, S. A., Hur, S. K., Seo, J. W. & Kwon, J. Stabilization and targeting of INO80 to replication forks by BAP1 during normal DNA synthesis. *Nat. Commun.* **5,** 5128 (2014).
16. Zarrizi, R., Menard, J. A., Belting, M. & Massoumi, R. Deubiquitination of γ-tubulin by BAP1 prevents chromosome instability in breast cancer cells. *Cancer Res.* **74,** 6499–6508 (2014).
17. Ismail, I. H. *et al.* Germline mutations in BAP1 impair its function in DNA double-strand break repair. *Cancer Res.* **74,** 4282–4294 (2014).
18. Yu, H. *et al.* Tumor suppressor and deubiquitinase BAP1 promotes DNA double-strand break repair. *Proc. Natl Acad. Sci. USA* **111,** 285–290 (2014).
19. Mashtalir, N. *et al.* Autodeubiquitination protects the tumor suppressor BAP1 from cytoplasmic sequestration mediated by the atypical ubiquitin ligase UBE2O. *Mol. Cell* **54,** 392–406 (2014).
20. Clapham, D. E. Calcium signaling. *Cell* **131,** 1047–1058 (2007).
21. Berridge, M. J. The inositol trisphosphate/calcium signaling pathway in health and disease. *Physiol. Rev.* **96,** 1261–1296 (2016).
22. Mikoshiba, K. The IP3 receptor/Ca^{2+} channel and its cellular function. *Biochem. Soc. Symp.* **74,** 9–22 (2007).
23. Palmer, A. E., Jin, C., Reed, J. C. & Tsien, R. Y. Bcl-2-mediated alterations in endoplasmic reticulum Ca^{2+} analyzed with an improved genetically encoded fluorescent sensor. *Proc. Natl Acad. Sci. USA* **101,** 17404–17409 (2004).
24. Giorgi, C. *et al.* Mitochondrial Ca^{2+} and apoptosis. *Cell Calcium* **52,** 36–43 (2012).
25. Giorgi, C. *et al.* PML regulates apoptosis at endoplasmic reticulum by modulating calcium release. *Science* **330,** 1247–1251 (2010).
26. Oberdorf, J., Webster, J. M., Zhu, C. C., Luo, S. G. & Wojcikiewicz, R. J. Down-regulation of types I, II and III inositol 1,4,5-trisphosphate receptors is mediated by the ubiquitin/proteasome pathway. *Biochem. J.* **339,** 453–461 (1999).
27. Mendes, C. C. *et al.* The type III inositol 1,4,5-trisphosphate receptor preferentially transmits apoptotic Ca^{2+} signals into mitochondria. *J. Biol. Chem.* **280,** 40892–40900 (2005).
28. Qi, F. *et al.* Continuous exposure to chrysotile asbestos can cause transformation of human mesothelial cells via HMGB1 and TNF-α signaling. *Am. J. Pathol.* **183,** 1654–1666 (2013).
29. Bhattacharya, S., Hanpude, P. & Maiti, T. K. Cancer associated missense mutations in BAP1 catalytic domain induce amyloidogenic aggregation: a new insight in enzymatic inactivation. *Sci. Rep.* **5,** 18462 (2015).
30. Wiesner, T. *et al.* Germline mutations in BAP1 predispose to melanocytic tumors. *Nat. Genet.* **43,** 1018–1021 (2011).

Supplementary Information is available in the online version of the paper.

Acknowledgements We are grateful to the members of the L and W families who donated their cells to our research. We acknowledge K. Dixon for advice on ultraviolet radiation studies, M. Pagano for advice on ubiquitylation assays, H. Yu for advice on DNA repair studies, I. Pagano for review of all statistical analyses, and G. Khan for technical support. This work was supported by grants National Cancer Institute (NCI) R01 CA198138 to M.C.; by NCI R01 CA160715, DOD CA120355 to H.Y.; by the University of Hawai'i Foundation, which received unrestricted donations to support mesothelioma research from Honeywell International, to M.C.; by The Riviera United 4-a Cure to M.C. and H.Y.; and by the Italian Association for Cancer Research (AIRC) (IG-18624, MFAG13521) and the Italian Ministry of Health to P.P. and C.G. P.P. thanks C. degli Scrovegni for support.

Author Contributions M.C. conceived the study. A.B. led the experiments and prepared the figures. M.C., S.Pas. and H.Y. built pedigrees. M.N. and M.T. genotyped patients and controls. P.M., G.S. and L.K.F. performed skin biopsies. A.B., C.G. and K.V. established fibroblast cell cultures. A.B., C.G., S.Pat. and V.S. independently conducted and reproduced cell death assays. D.L. performed flow cytometry experiments. A.R. and C.T. performed electron microscopy studies. A.B. and C.G. performed subcellular fractionation studies. A.B. performed western blot, co-immunoprecipitation, aequorin-based Ca^{2+} measurements, and *in vitro* cell transformation assays. C.G. and S.Pat. performed single-cell Ca^{2+} measurements. C.G., S.Pat. and F.O. performed immunofluorescence studies. A.D. performed proximity ligation assay studies. A.B., with the help of S.K., performed ubiquitylation assays. L.P. performed qRT–PCR studies. A.B., C.G. and S.Pat., with the help of E.B.A., performed ionizing radiation and ultraviolet radiation studies. A.N., S.Pas., G.G. and H.I.P. discussed the results. M.C., H.Y. and P.P. coordinated the study and oversaw the results. A.B. and M.C. wrote the manuscript with help from co-authors.

Author Information Reprints and permissions information is available at www.nature.com/reprints. The authors declare competing financial interests: details are available in the online version of the paper. Readers are welcome to comment on the online version of the paper. Publisher's note: Springer Nature remains neutral with regard to jurisdictional claims in published maps and institutional affiliations. Correspondence and requests for materials should be addressed to M.C. (MCarbone@cc.hawaii.edu), P.P. (paolo.pinton@unife.it), or H.Y. (HYang@cc.hawaii.edu).

Reviewer Information *Nature* thanks M. Campanella, N. Hayward, K. D. Wilkinson and the other anonymous reviewer(s) for their contribution to the peer review of this work.

METHODS

Subjects. *BAP1*$^{+/-}$ mutant carriers and unaffected controls were recruited from the L and W families; they donated the skin biopsies from which we derived the fibroblast cell cultures studied here. In previous studies, we demonstrated that around 50% of L and W family members inherited heterozygous *BAP1* mutations[5]. Except for being adult members of these two families, no other predefined inclusion/exclusion criteria were applied. Written informed consent was received from all participants (*BAP1*$^{+/-}$ mutant carriers, and gender- and age-matched unaffected family members). Collection and use of patient information and samples were approved by the Institutional Review Board of the University of Hawaii (protocol number 14406). Germline *BAP1* sequencing was conducted on genomic DNA extracted from peripheral blood using standard methods and analysed by bidirectional sequencing of the *BAP1* gene in the Hawaii Cancer Consortium Queen Medical Center CLIA/CAP certified laboratory, as described[5]. Fourteen family members (seven *BAP1*^{WT} and seven *BAP1*$^{+/-}$) volunteered their skin biopsies for these studies and they were matched by gender and age. Assuming a two-tailed type I error rate (alpha) equal to 0.05 and seven observations per group (14 total), we had 80% power to detect a standardized difference equal to 1.8. Since we found a statistical difference, we had sufficient power to detect a pre-specified effect size.

Primary cultures of human dermal fibroblasts were established in tissue culture from biopsies of sun-protected forearm skin from donors of different gender and age. Biopsies were taken using a 5 mm punch (Schuco) on skin site previously disinfected and anaesthetized[31].

Cell cultures. We derived human dermal skin fibroblasts from explants of skin biopsies from four *BAP1*^{WT} and four *BAP1*$^{+/-}$ Wisconsin (W) family members, and three *BAP1*^{WT} and three *BAP1*$^{+/-}$ Louisiana (L) family members. Fibroblasts were grown from these skin explants and cultured in Dulbecco modified Eagle's medium (DMEM) with glucose (4.5 g l^{-1}), 2 mM L-glutamine, without sodium pyruvate (Corning Cellgro), supplemented with 10% (v/v) fetal bovine serum (FBS) (Gibco) and 1% penicillin–streptomycin[31]. All the experiments were performed on fibroblasts between tissue culture passages 7 and 15.

Primary human mesothelial cells. We routinely established human mesothelial cells in tissue culture from pleural fluids that accumulated in individuals with congestive heart failure or other non-malignant conditions, who provided written informed consent. Human mesothelial cells were characterized by immunohistochemistry and cultured in DMEM with 20% FBS, as previously described[32]. Independent human mesothelial cells cultures from three different donors between tissue culture passages 4 and 5 were used in the experiments described here; each experiment for each of these human mesothelial cell cultures was conducted in triplicate.

Malignant mesothelioma cell lines. PPM-Mill, Phi, HMESO, Rob[33] (established and provided by H.I.P.), and human embryonic kidney cells (HEK293, provided by P.P.) were grown in DMEM supplemented with 10% FBS and 1% penicillin–streptomycin. HMESO stable clones were generated as described below (see 'Gene silencing with siRNA, adenovirus-mediated gene transfer, and transfection'), and grown in DMEM with glucose (4.5 g l^{-1}), 2 mM L-glutamine, without sodium pyruvate (Corning Cellgro), supplemented with 10% (v/v) FBS (Gibco), 1% penicillin–streptomycin, and 0.5 mg ml^{-1} G418 (Geneticin). THP-1 cells (human monocytic cell line from acute monocytic leukaemia,) were obtained from the American Type Culture Collection (ATCC) and cultured in RPMI-1640 Medium (Corning Cellgro) supplemented with 10% (v/v) FBS (Gibco) and 1% penicillin–streptomycin; treatment with 20 μM 12-*O*-tetradecanoylphorbol 13-acetate (TPA) for 24 h was performed to induce monocyte differentiation into macrophages[34]. MAF cell cultures were derived from 3-month-old *Bap1*^{WT} and *Bap1*$^{+/-}$ mice[35] genotyped as described[35]; MAFs were grown in DMEM supplemented with 10% FBS and 1% penicillin–streptomycin. Cells were cultured in a humidified atmosphere of 5% (v/v) carbon dioxide in air at 37 °C. All cells used in the experiments reported here were routinely tested for mycoplasma contamination (about once a month) using a LookOut Mycoplasma PCR Detection Kit (Sigma-Aldrich, catalogue number MP0035) and were confirmed to be mycoplasma-free.

All main experiments were conducted in primary cells from human volunteers (fibroblasts and human mesothelial cells). Therefore, the results are related to the reduced levels of BAP1 present in cells derived from carriers of heterozygous germline *BAP1* mutations and to the reduced levels of BAP1 we induced in primary human mesothelial cells by siRNA. In other words, the results presented could not be influenced by the numerous genetic alterations that are found in tumour-derived cell lines. Some confirmatory experiments were conducted in cell lines. None of the cell lines used in this paper were found in the International Cell Line Authentication Committee or National Center for Biotechnology Information Biosample databases of misidentified cell lines. Short-tandem repeat analyses were performed upon arrival of these cell lines in our laboratory for authentication. Re-authentication of the cell lines confirming their identity was performed by 'Genetica DNA Laboratories, LabCorp' in July 2015.

Growth curves. Fibroblast cell culture proliferation was measured using an AlamarBlue assay (AbD Serotec, catalogue number BUF012B). After incubation of the cells in 96-well plates, 10% v/v AlamarBlue was added and fluorescence was measured (excitation 560 nm, emission 590 nm) at the indicated time points.

Gene silencing with siRNA, adenovirus-mediated gene transfer, and transfection. siRNA oligonucleotides were obtained from Qiagen. GeneSoluton siRNAs targeting four different BAP1 mRNAs were as follows: Hs_BAP1_1, catalogue number SI00066696; Hs_BAP1_2, catalogue number SI00066703; Hs_BAP1_3, catalogue number SI00066710; Hs_BAP1_5, catalogue number SI03036390. GeneSoluton siRNAs targeting four different IP3R3 mRNAs (ITPR3) were as follows: Hs_ITPR3_1, catalogue number SI00034580; Hs_ ITPR3_2, catalogue number SI00034587; Hs_ ITPR3_3, catalogue number SI00034594; Hs_ ITPR3_4, catalogue number SI00034601. Negative control siRNA was catalogue number 1027280. Transfection was performed with HiPerfect (Qiagen), using siRNAs at 10 nM final concentrations in 0.1% FBS medium for 24 h. Unless otherwise specified in the figures, a pool of the four different siRNAs, listed above, was used to silence BAP1 or IP3R3.

Adenoviruses expressing BAP1 and GFP were purchased from SignaGen Laboratories (Ad-BAP1, catalogue number SL175127; Ad-GFP, catalogue number SL100708). Customized adenoviruses expressing Ad-Myc–BAP1, Ad-Myc–BAP1(C91S), Ad-Myc–BAP1(W), and Ad-Myc–BAP1(L) were produced by SignaGen Laboratories using their Ad.MAX System. Expression plasmids for Flag–HA–BAP1, Myc–BAP1, Myc–BAP1(W), Myc–BAP1(L), and Myc–BAP1(C91S) were produced by Blue Heron Biotech. For BAP1(W), BAP1(L), and BAP1(C91S), the following nucleotide sequences were used.

BAP1(W): ATGAATAAGGGCTGGCTGGAGCTGGAGAGCGACCCAG
GCCTCTTCACCCTGCTCGTGGAAGATTTCGGTGTCAAGGGGGTGCAAG
TGGAGGAGATCTACGACCTTCAGAGCAAATGTCAGGGCCCTGTATATG
GATTTATCTTCCTGTTCAAATGGATCGAAGAGCGCCGGTCCCGGCGAA
AGGTCTCTACCTTGGTGGATGATACGTCCGTGATTGATGATGATATTGT
GAATAACATGTTCTTTGCCCACCAGCTGATACCCAACTCTTGTGCAAC
TCATGCCTTGCTGAGCGTGCTCCTGAACTGCAGCAGCGTGGACCTGG
GACCCACCCTGAGTCGCATGAAGGACTTCACCAAGGGTTTCAGCCCT
GAGAGCAAAGGATATGCGATTGGCAATGCCCCGGAGTTGGCCAAGGC
CCATAATAGCCATGCCAGGGCCCTGGGGGGGAGGACGAGGAGT GGACAG
ACAAGGCCCGGCGGGTCATCATGGAGCGTATCGGCCTCGCCACTGCA
GGGGAGCCCTACCACGACATCCGCTTCAACCTGATGGCAGTGGTGCC
CGACCGCA GGATCAAGTATGA.

BAP1(L): ATGAATAAGGGCTGGCTGGAGCTGGAGAGCGACCCAG
GCCTCTTCACCCTGCTCGTGGAAGATTTCGGTGTCAAGGGGGTGCAA
GTGGAGGAGATCTACGACCTTCAGAGCAAATGTCAGGGCCCTGTATAT
GGATTTATCTTCCTGTTCAAATGGATCGAAGAGCGCCGGTCCCGGCGA
AAGGTCTCTACCTTGGTGGATGATACGTCCGTGATTGATGATGATATTG
TGAATAACATGTTCTTTGCCCACCAGCTGATACCCAACTCTTGTGCAAC
TCATGCCTTGCTGAGCGTGCTCCTGAACTGCAGCAGCGTGGACCTGGG
ACCCACCCTGAGTCGCATGAAGGACTTCACCAAGGGTTTCAGCCCTG
AGAGCAAAGGATATGCGATTGGCAATGCCCCGGAGTTGGCCAAGGCC
CATAATAGCCATGCCAGGCCCGAGCCACGCCCACCTCCCTGAGAAGCA
GAATGGCCTTAGTGCAGTGCGGACCATGGAGGCGTTCCACTTTGTCAG
CTATGTGCCTATCACAGGCCGGCTCTTTGAGCTGGATGGGCTGAAGGT
CTACCCCATTGACCATGGGCCCTGGGGGGAGGACGAGGAGTGGACAG
ACAAGGCCCGGCGGGTCATCATGGAGCGTATCGGCCTCGCCACTGCA
GGGGAGCCCTACCACGACATCCGCTTCAACCTGATGGCAGTGGTGCC
CGACCGCAGGATCAAGTATGAGGCCAGGCTGCATGTGCTGAAGGTGA
ACCGTCAGACAGTACTAGAGGCTCTGCAGCAGCTGATAAGAGTAACAC
AGCCAGAGCTGATTCAGACCCACAAGTCTCAAGAGTCACAGCTGCCTG
AGGAGTCCAAGTCAGCCAGCAACAAGTCCCCGCTGGTGCTGGAAGCAA
ACAGGGCCCCTGCAGCCTCTGAGGGCAACCACACAGATGGTGCAGAGG
AGGCGGCTGGTTCATGCGCACAAGCCCCATCCCACAGCCCTCCCAACA
AACCCAAGCTAGTGGTGAAGCCTCCAGGCAGCAGCCTCAATGGGGTTC
ACCCCAACCCCACTCCCATTGTCCAGCGGCTGCCGGCCTTTCTAGACA
ATCACAATTATGCCAAGTCCCCCATGCAGGAGGAAGAAGACCTGGCGG
CAGGTGTGGGCCGCAGCCGAGTTCCAGTCCGCCCACCCCAGCAGTACT
CAGATGATGAGGATGACTATGAGGATGACGAGGAGGATGACGTGCAGA
ACACCAACTCTGCCCTTAGGTATAAGGGGAAGGGAACAGGGAAGCCAG
GGGCATTGAGCGGTTCTGCTGATGGGCAACTGTCAGTGCTGCAGCCCA
ACACCATCAACGTCTTGGCTGAGAAGCTCAAAGAGTCCCAGAAGGACC
TCTCAATTCCTCTGTCCATCAAGACTAGCAGCGGGGCTGGGAGTCCGG
CTGTGGCAGTGCCCACACACTCGCAGCCCTCACCCACCCCCAGCAATG
AGAGTACAGACACGGCCTCTGAGATCGGCAGTGCTTTCAACTCGCCAC

TGCGCTCGCCTATCCGCTCAGCCAACCCGACGCGGCCCTCCAGCCCTG
TCACCTCCCACATCTCCAAGGTGCTTTTTGGAGAGGATGACAGCCTGC
TGCGTGTTGACTGCATACGCTACAACCGTGCTGTCCGTGATCTGGGTC
CTGTCATCAGCACAGGCCTGCTGCACCTGGCTGAGGATGGGGTGCTGA
GTCCCCTGGCGCTGACAGAGGGTGGGAAGGGTTCCTCGCCCTCCATCA
GACCAATCCAAGGCAGCCAGGGGTCCAGCAGCCCAGTGGAGAAGGAG
GTCGTGGAAGCCACGGACAGCAGAGAGAAGACGGGGATGGTGAGGC
CTGGCGAGCCCTTGAGTGGGGAGAAATACTCACCCAAGGAGCTGCTGG
CACTGCTGAAGTGTGTGGAGGCTGAGATTGCAAACTATGAGGCGTGCCT
CAAGGAGGAGGTAGAGAAGAGGAAGAAGTTCAAGATTGATGACCAGAG
AAGGACCCACAACTACGATGAGTTCATCTGCACCTTTATCTCCATGCTG
GCTTAG.

BAP1(C91S): ATGAATAAGGGCTGGCTGGAGCTGGAGAGCGACC
CAGGCCTCTTCACCCTGCTCGTGGAAGATTTCGGTGTCAAGGGGGTGC
AAGTGGAGGAGATCTACGACCTTCAGAGCAAATGTCAGGGCCCTGTATA
TGGATTTATCTTCCTGTTCAAATGGATCGAAGAGCGCCGGTCCCGGCGA
AAGGTCTCTACCTTGGTGGATGATACGTCCGTGATTGATGATGATATTG
TGAATAACATGTTCTTTGCCCACCAGCTGATACCCAACTCTAGTGCAAC
TCATGCCTTGCTGAGCGTGCTCCTGAACTGCAGCAGCGTGGACCTGGG
ACCCACCCTGAGTCGCATGAAGGACTTCACCAAGGGTTTCAGCCCTGA
GAGCAAAGGATATGCGATTGGCAATGCCCCGGAGTTGGCCAAGGCCCA
TAATAGCCATGCCAGGCCCGAGCCACGCCACCTCCCTGAGAAGCAGAA
TGGCCTTAGTGCAGTGCGGACCATGGAGGCGTTCCACTTTGTCAGCTAT
GTGCCTATCACAGGCCGGCTCTTTGAGCTGGATGGGCTGAAGGTCTAC
CCCATTGACCATGGGCCCTGGGGGGAGGACGAGGAGTGGACAGACAA
GGCCCGGCGGGTCATCATGGAGCGTATCGGCCTCGCCACTGCAGGGGA
GCCCTACCACGACATCCGCTTCAACCTGATGGCAGTGGTGCCCGACCGC
AGGATCAAGTATGAGGCCAGGCTGCATGTGCTGAAGGTGAACCGTCAG
ACAGTACTAGAGGCTCTGCAGCAGCTGATAAGAGTAACACAGCCAGAG
CTGATTCAGACCCACAAGTCTCAAGAGTCACAGCTGCCTGAGGAGTCC
AAGTCAGCCAGCAACAAGTCCCCGCTGGTGCTGGAAGCAAACAGGGC
CCCTGCAGCCTCTGAGGGCAACCACACAGATGGTGCAGAGGAGGCGGC
TGGTTCATGCGCACAAGCCCCATCCCACAGCCCTCCCAACAAACCCAA
GCTAGTGGTGAAGCCTCCAGGCAGCAGCCTCAATGGGGTTCACCCCA
ACCCCACTCCCATTGTCCAGCGGCTGCCGGCCTTTCTAGACAATCACAA
TTATGCCAAGTCCCCCATGCAGGAGGAAGAAGACCTGGCGGCAGGTG
TGGGCCGCAGCCGAGTTCCAGTCCGCCCACCCCAGCAGTACTCAGATG
ATGAGGATGACTATGAG GATGACGAGGAGGATGACGTGCAGAACA
CCAACTCTGCCCTTAGGTATAAGGGGAAGGGAACAGGGAAGCCAGGG
GCATTGAGCGGTTCTGCTGATGGGCAACTGTCAGTGCTGCAGCCCAAC
ACCATCAACGTCTTGGCTGAGAAGCTCAAAGAGTCCCAGAAGGACCT
CTCAATTCCTCTGTCCATCAAGACTAGCAGCGGGGCTGGGAGTCCGGC
TGTGGCAGTGCCCACACACTCGCAGCCCTCACCCACCCCCAGCAATGAG
AGTACAGACACGGCCTCTGAGATCGGCAGTGCTTTCAACTCGCCACTGC
GCTCGCCTATCCGCTCAGCCAACCCGACGCGGCCCTCCAGCCCTGTCA
CCTCCCACATCTCCAAGGTGCTTTTTGGAGAGGATGACAGCCTGCTGC
GTGTTGACTGCATACGCTACAACCGTGCTGTCCGTGATCTGGGTCCTG
TCATCAGCACAGGCCTGCTGCACCTGGCTGAGGATGGGGTGCTGAGTC
CCCTGGCGCTGACAGAGGGTGGGAAGGGTTCCTCGCCCTCCATCAGAC
CAATCCAAGGCAGCCAGGGGTCCAGCAGCCCAGTGGAGAAGGAGGTC
GTGGAAGCCACGGACAGCAGAGAGAAGACGGGGATGGTGAGGCCTGG
CGAGCCCTTGAGTGGGGAGAAATACTCACCCAAGGAGCTGCTGGCACT
GCTGAAGTGTGTGGAGGCTGAGATTGCAAACTATGAGGCGTGCCTCAA
GGAGGAGGTAGAGAAGAGGAAGAAGTTCAAGATTGATGACCAGAGAAG
GACCCACAACTACGATGAGTTCATCTGCACCTTTATCTCCATGCTGGCT
CAGGAAGGCATGCTGGCCAACCTAGTGGAGCAGAACATCTCCGTGCGG
CGGCGCCAAGGGGTCAGCATCGGCCGGCTCCACAAGCAGCGGAAGCCT
GACCGGCGGAAACGCTCTCGCCCCTACAAGGCCAAGCGCCAGTGA.

Customized adenoviruses expressing Ad-Myc–BAP1-ER, Ad-Myc–BAP1-Nu, and Ad-Myc–BAP1-Cyt were produced by SignaGen Laboratories. The respective expression plasmids were produced by Blue Heron Biotech. The following nucleotide sequences were used and cloned into the expression vector pCMV6-AN-My (catalogue number PS100012).

BAP1-ER: ATGAATAAGGGCTGGCTGGAGCTGGAGAGCGACCCAGG
CCTCTTCACCCTGCTCGTGGAAGATTTCGGTGTCAAGGGGGTGCAA GT
GGAGGAGATCTACGACCTTCAGAGCAAATGTCAGGGCCCTGTATATGGA
TTTATCTTCCTGTTCAAATGGATCGAAGAGCGCCGGTCCCGGCGAAAG
GTCTCTACCTTGGTGGATGATACGTCCGTGATTGATGATGATATTGTGAA
TAACATGTTCTTTGCCCACCAGCTGATACCCAACTCTTGTGCAACTCAT
GCCTTGCTGAGCGTGCTCCTGAACTGCAGCAGCGTGGACCTGGGACCC
ACCCTGAGTCGCATGAAGGACTTCACCAAGGGTTTCAGCCCTGAGAGC
AAAGGATATGCGATTGGCAATGCCCCGGAGTTGGCCAAGGCCCATAAT
AGCCATGCCAGGCCCGAGCCACGCCACCTCCCTGAGAAGCAGAATGG
CCTTAGTGCAGTGCGGACCATGGAGGCGTTCCACTTTGTCAGCTATGTG
CCTATCACAGGCCGGCTCTTTGAGCTGGATGGGCTGAAGGTCTACCCCA
TTGACCATGGGCCCTGGGGGGAGGACGAGGAGTGGACAGACAAGGCC
CGGCGGGTCATCATGGAGCGTATCGGCCTCGCCACTGCAGGGGAGCC
CTACCACGACATCCGCTTCAACCTGATGGCAGTGGTGCCCGACCGCAG
GATCAAGTATGAGGCCAGGCTGCATGTGCTGAAGGTGAACCGTCAGAC
AGTACTAGAGGCTCTGCAGCAGCTGATAAGAGTAACACAGCCAGAGCT
GATTCAGACCCACAAGTCTCAAGAGTCACAGCTGCCTGAGGAGTCCAA
GTCAGCCAGCAACAAGTCCCCGCTGGTGCTGGAAGCAAACAGGGCCCC
TGCAGCCTCTGAGGGCAACCACACAGATGGTGCAGAGGAGGCGGCTG
GTTCATGCGCACAAGCCCCATCCCACAGCCCTCCCAACAAACCCAAGC
TAGTGGTGAAGCCTCCAGGCAGCAGCCTCAATGGGGTTCACCCCAACC
CCACTCCCATTGTCCAGCGGCTGCCGGCCTTTCTAGACAATCACAATT
ATGCCAAGTCCCCCATGCAGGAGGAAGAAGACCTGGCGGCAGGTGTGG
GCCGCAGCCGAGTTCCAGTCCGCCCACCCCAGCAGTACTCAGATGATG
AGGATGACTATGAGGATGACGAGGAGGATGACGTGCAGAACACCAAC
TCTGCCCTTAGGTATAAGGGGAAGGGAACAGGGAAGCCAGGGGCATTG
AGCGGTTCTGCTGATGGGCAACTGTCAGTGCTGCAGCCCAACACCATC
AACGTCTTGGCTGAGAAGCTCAAAGAGTCCCAGAAGGACCTCTCAATT
CCTCTGTCCATCAAGACTAGCAGCGGGGCTGGGAGTCCGGCTGTGGCA
GTGCCCACACACTCGCAGCCCTCACCCACCCCCAGCAATGAGAGTACA
GACACGGCCTCTGAGATCGGCAGTGCTTTCAACTCGCCACTGCGCTCG
CCTATCCGCTCAGCCAACCCGACGCGGCCCTCCAGCCCTGTCACCTCC
CACATCTCCAAGGTGCTTTTTGGAGAGGATGACAGCCTGCTGCGTGTT
GACTGCATACGCTACAACCGTGCTGTCCGTGATCTGGGTCCTGTCATC
AGCACAGGCCTGCTGCACCTGGCTGAGGATGGGGTGCTGAGTCCCCT
GGCGCTGACAGAGGGTGGGAAGGGTTCCTCGCCCTCCATCAGACCAA
TCCAAGGCAGCCAGGGGTCCAGCAGCCCAGTGGAGAAGGAGGTCG TG
GAAGCCACGGACAGCAGAGAGAAGACGGGGATGGTGAGGCCTGGCGA
GCCCTTGAGTGGGGAGAAATACTCACCCAAGGAGCTGCTGGCACTGCT
GAAGTGTGTGGAGGCTGAGATTGCAAACTATGAGGCGTGCCTCAAGG
AGGAGGTAGAGAAGAGGAAGAAGTTCAAGATTGATGACCAGAGAAGG
ACCCACAACTACGATGAGTTCATCTGCACCTTTATCTCCATGCTGGCT
CAGGAAGGCATGCTGGCCAACCTAGTGGAGCAGAACATCTCCGTGCG
GCGGCGCCAAGGGGTCAGCATCGGCCGGCTCCACAAGCAGCGGAAGC
CTGACCGGCGGAAACGCTCTCGCCCCTACAAGGCCAAGCGCCAGATG
GTTTATATTGGTATCGCTATTTTTTTGTTTTTGGTTGGCCTTTTTATGA
AATGA.

ER targeting sequence: ATGGTTTATATTGGTATCGCTATTTTTTTG
TTTTTGGTTGGCCTTTTTATGAAA.

BAP1-Nu: ATGAATAAGGGCTGGCTGGAGCTGGAGAGCGACCCAG
GCCTCTTCACCCTGCTCGTGGAAGATTTCGGTGTCAAGGGGGTGCAAG
TGGAGGAGATCTACGACCTTCAGAGCAAATGTCAGGGCCCTGTATATG
GATTTATCTTCCTGTTCAAATGGATCGAAGAGCGCCGGTCCCGGCGAAA
GGTCTCTACCTTGGTGGATGATACGTCCGTGATTGATGATGATATTGTG
AATAACATGTTCTTTGCCCACCAGCTGATACCCAACTCTTGTGCAACTC
ATGCCTTGCTGAGCGTGCTCCTGAACTGCAGCAGCGTGGACCTGGGAC
CCACCCTGAGTCGCATGAAGGACTTCACCAAGGGTTTCAGCCCTGAGA
GCAAAGGATATGCGATTGGCAATGCCCCGGAGTTGGCCAAGGCCCATA
ATAGCCATGCCAGGCCCGAGCCACGCCACCTCCCTGAGAAGCAGAATG
GCCTTAGTGCAGTGCGGACCATGGAGGCGTTCCACTTTGTCAGCTATG
TGCCTATCACAGGCCGGCTCTTTGAGCTGGATGGGCTGAAGGTCTACC
CCATTGACCATGGGCCCTGGGGGGAGGACGAGGAGTGGACAGACAAG
GCCCGGCGGGTCATCATGGAGCGTATCGGCCTCGCCACTGCAGGGGAG
CCCTACCACGACATCCGCTTCAACCTGATGGCAGTGGTGCCCGACCGCA
GGATCAAGTATGAGGCCAGGCTGCATGTGCTGAAGGTGAACCGTCAGA
CAGTACTAGAGGCTCTGCAGCAGCTGATAAGAGTAACACAGCCAGAGC
TGATTCAGACCCACAAGTCTCAAGAGTCACAGCTGCCTGAGGAGTCCA
AGTCAGCCAGCAACAAGTCCCCGCTGGTGCTGGAAGCAAACAGGGCC
CCTGCAGCCTCTGAGGGCAACCACACAGATGGTGCAGAGGAGGCGGC
TGGTTCATGCGCACAAGCCCCATCCCACAGCCCTCCCAACAAACCCAA
GCTAGTGGTGAAGCCTCCAGGCAGCAGCCTCAATGGGGTTCACCCCAA
CCCCACTCCCATTGTCCAGCGGCTGCCGGCCTTTCTAGACAATCACAA
TTATGCCAAGTCCCCCATGCAGGAGGAAGAAGACCTGGCGGCAGGTGT
GGGCCGCAGCCGAGTTCCAGTCCGCCCACCCCAGCAGTACTCAGATGA
TGAGGATGACTATGAGGATGACGAGGAGGATGACGTGCAGAACACCAA
CTCTGCCCTTAGGTATAAGGGGAAGGGAACAGGGAAGCCAGGGGCAT
TGAGCGGTTCTGCTGATGGGCAACTGTCAGTGCTGCAGCCCAACACCA
TCAACGTCTTGGCTGAGAAGCTCAAAGAGTCCCAGAAGGACCTCTCAA
TTCCTCTGTCCATCAAGACTAGCAGCGGGGCTGGGAGTCCGGCTGTGG
CAGTGCCCACACACTCGCAGCCCTCACCCACCCCCAGCAATGAGAGTA

CAGACACGGCCTCTGAGATCGGCAGTGCTTTCAACTCGCCACTGCGCT
CGCCTATCCGCTCAGCCAACCCGACGCGGCCCTCCAGCCCTGTCACCT
CCCACATCTCCAAGGTGCTTTTTGGAGAGGATGACAGCCTGCTGCGTG
TTGACTGCATACGCTACAACCGTGCTGTCCGTGATCTGGGTCCTGTCA
TCAGCACAGGCCTGCTGCACCTGGCTGAGGATGGGGTGCTGAGTCCC
CTGGCGCTGACAGAGGGTGGGAAGGGTTCCTCGCCCTCCATCAGACCA
ATCCAAGGCAGCCAGGGGTCCAGCAGCCCAGTGGAGAAGGAGGTCGTG
GAAGCCACGGACAGCAGAGAGAAGACGGGGATGGTGAGGCCTGGCG
AGCCCTTGAGTGGGGAGAAATACTCACCCAAGGAGCTGCTGGCACTG
CTGAAGTGTGTGGAGGCTGAGATTGCAAACTATGAGGCGTGCCTCAAG
GAGGAGGTAGAGAAGAGGAAGAAGTTCAAGATTGATGACCAGAGAAG
GACCCACAACTACGATGAGTTCATCTGCACCTTTATCTCCATGCTGGCT
CAGGAAGGCATGCTGGCCAACCTAGTGGAGCAGAACATCTCCGTGCG
GCGGCGCCAAGGGGTCAGCATCGGCCGGCTCCACAAGCAGCGGAAGC
CTGACCGGCGGAAACGCTCTCGCCCCTACAAGGCCAAGCGCCAG<u>ACA
GTTTTTTCTAATGGCTATTCAAGCCCCAGCATGAGACCAGATGTAAGCT
CTCCTCCATCCAGCTCCTCAACAGCAACAACAGGACCACCTCCCAAAC
TCTGCCTGGTGTGCTCTGATGAAGCTTCAGGATGTCATTATGGAGTCT
TAACTTGTGGAAGCTGTAAAGTTTTCTTCAAAAGAGCAGTGGAAGGACA
GCACAATTACCTATGTGCTGGAAGGAATGATTGCATCATCGATAAAATT
CGAAGAAAAAACTGCCCAGCATGCCGCTATCGAAAATGTCTTCAGGCT
GGAATGAACCTGGAAGCTCGAAAAACAAAGAAAAAAATAAAAGGAAT
TCAGCAGGCCACT</u>TGA.

Nuclear targeting sequence: ACAGTTTTTTCTAATGGCTATTCAAG
CCCCAGCATGAGACCAGATGTAAGCTCTCCTCCATCCAGCTCCTCAAC
AGCAACAACAGGACCACCTCCCAAACTCTGCCTGGTGTGCTCTGATGA
AGCTTCAGGATGTCATTATGGAGTCTTAACTTGTGGAAGCTGTAAAGT
TTTCTTCAAAAGAGCAGTGGAAGGACAGCACAATTACCTATGTGCTGG
AAGGAATGATTGCATCATCGATAAAATTCGAAGAAAAAACTGCCCAGCA
TGCCGCTATCGAAAATGTCTTCAGGCTGGAATGAACCTGGAAGCTCGA
AAAACAAAGAAAAAAATAAAAGGAATTCAGCAGGCCACT.

BAP1-Cyt: ATGAATAAGGGCTGGCTGGAGCTGGAGAGCGACCCAG
GCCTCTTCACCCTGCTCGTGGAAGATTTCGGTGTCAAGGGGGTGCAA
GTGGAGGAGATCTACGACCTTCAGAGCAAATGTCAGGGCCCTGTATAT
GGATTTATCTTCCTGTTCAAATGGATCGAAGAGCGCCGGTCCCGGCGA
AAGGTCTCTACCTTGGTGGATGATACGTCCGTGATTGATGATGATATTG
TGAATAACATGTTCTTTGCCCACCAGCTGATACCCAACTCTTGTGCAAC
TCATGCCTTGCTGAGCGTGCTCCTGAACTGCAGCAGCGTGGACCTGG
GACCCACCCTGAGTCGCATGAAGGACTTCACCAAGGGTTTCAGCCCT
GAGAGCAAAGGATATGCGATTGGCAATGCCCCGGAGTTGGCCAAGGC
CCATAATAGCCATGCCAGGCCCGAGCCACGCCACCTCCCTGAGAAGCA
GAATGGCCTTAGTGCAGTGCGGACCATGGAGGCGTTCCACTTTGTCAG
CTATGTGCCTATCACAGGCCGGCTCTTTGAGCTGGATGGGCTGAAGGT
CTACCCCATTGACCATGGGCCCTGGGGGGAGGACGAGGAGTGGACAG
ACAAGGCCCGGCGGGTCATCA TGGAGCGTATCGGCCTCGCCACTGC
AGGGGAGCCCTACCACGACATCCGCTTCAACCTGATGGCAGTGGTGCC
CGACCGCAGGATCAAGTATGAGGCCAGGCTGCATGTGCTGAAGGTGAA
CCGTCAGACAGTACTAGAGGCTCTGCAGCAGCTGATAAGAGTAACACA
GCCAGAGCTGATTCAGACCCACAAGTCTCAAGAGTCACAGCTGCCTGA
GGAGTCCAAGTCAGCCAGCAACAAGTCCCCGCTGGTGCTGGAA GCAA
ACAGGGCCCCTGCAGCCTCTGAGGGCAACCACACAGATGGTGCAGAGG
AGGCGGCTGGTTCATGCGCACAAGCCCCATCCCACAGCCCTCCCAAC
AAACCCAAGCTAGTGGTGAAGCCTCCAGGCAGCAGCCTCAATGGGGT
TCACCCCAACCCCACTCCCATTGTCCAGCGGCTGCCGGCCTTTCTAGAC
AATCACAATTATGCCAAGTCCCCCATGCAGGAGGAAGAAGACCTGGCG
GCAGGTGTGGGCCGCAGCCGAGTTCCAGTCCGCCCACCCCAGCAGTA
CTCAGATGATGAGGATGACTATGAGGATGACGAGGAGGATGACGTGCA
GAACACCAACTCTGCCCTTAGGTATAAGGGGAAGGGAACAGGGAAGC
CAGGGGCATTGAGCGGTTCTGCTGATGGGCAACTGTCAGTGCTGCAG
CCCAACACCATCAACGTCTTGGCTGAGAAGCTCAAAGAGTCCCAGAAG
GACCTCTCAATTCCTC TGTCCATCAAGACTAGCAGCGGGGCTGG
GAGTCCGGCTGTGGCAGTGCCCACACACTCGCAGCCCTCACCCACCCC
CAGCAATGAGAGTACAGACACGGCCTCTGAGATCGGCAGTGCTTTCAA
CTCGCCACTGCGCTCGCCTATCCGCTCAGCCAACCCGACGCGGCCCTC
CAGCCCTGTCACCTCCCACATCTCCAAGGTGCTTTTTGGAGAGGATGA
CAGCCTGCTGCGTGTTGACTGCATACGCTACAACCGTGCTGTCCGTGA
TCTGGGTCCTGTCATCAGCACAGGCCTGCTGCACCTGGCTGAGGATGG
GGTGCTGAGTCCCCTGGCGCTGACAGAGGGTGGGAAGGGTTCCTCGCC
CTCCATCAGACCAATCCAAGGCAGCCAGGGGTCCAGCAGCCCAGTGGA
GAAGGAGGTCGTGGAAGCCACGGACAGCAGAGAGAAGACGGGGATGG
TGAGGCCTGGCGAGCCCTTGAGTGGGGAGAAATACTCACCCAAGGAGC
TGCTGGCACTGCTGAAGTGTGTGGAGGCTGAGATTGCAAACTATGAGG
CGTGCCTCAAGGAGGAGGTAGAGAAGAGGAAGAAGTTCAAGATTGATG
ACCAGAGAAGGACCCACAACTACGATGAGTTCATCTGCACCTTTATCT
CCATGCTGGCTCAGGAAGGCATGCTGGCCAACCTAGTGGAGCAGAACA
TCTCCGTG<u>GCGGCGGCGCAAGGGGTCAGCATCGGCGCGCTCCACAAGC
AGCGGAAGCCTGACGCGGCGGCGGCGGCGGCGCCCTAC</u>AAGGCCAA
GCGCCAGTGA.

Point mutations (in bold type) introduced in the BAP1 NLS region (according to ref. 19): **GCG**GCG**GCG**CAAGGGGTCAGCATCGGC**GC**GCTCCACAAGC
AGCGGAAGCCTGAC**GCG**GCG**GCGGCGGC**G**GGCG**CCCTAC.

The customized adenovirus expressing Ad-IP3R3 was produced by Vector BioLabs, from the expression plasmid ITPR3 (Myc–DDK-tagged)-Human inositol 1,4,5-trisphosphate receptor, type 3, obtained from Blue Heron Biotech (catalogue number RC222737).

The adenoviruses expressing Ad-cytAEQ, Ad-mtAEQ, and Ad-mtAEQmut were obtained from the laboratory of P.P.[36].

Plasmids expressing Flag–IP3R3(NT), HA–IP3R3(NT), HA–IP3R3(MID), and HA–IP3R3(CT) were generated by S.K.

Blue Heron Biotech produced the plasmid DNA vectors expressing the six Myc-tagged BAP1 fragments: Myc–BAP1(UCH), amino acids 1–240; Myc BAP1(NORS), amino acids 240–598, Myc–BAP1(CTD–NLS), amino acids 598–729; Myc–BAP1(UCH–NORS-CTD), amino acids 1–699; Myc–BAP1(UCH–NORS), amino acids 1–598; Myc–BAP1(NORS–CTD–NLS), amino acids 240–729.

Cells (fibroblast cell cultures, human mesothelial cells, MAFs, Phi, HMESO, macrophages, as indicated in the figures) were seeded and allowed to grow to 50% confluence for 24 h before transduction or transfection. Infection with the indicated adenoviruses was performed at a multiplicity of infection of 100 plaque-forming units per cell, in 10% FBS. For aequorin measurements, the cells were seeded onto 13 mm glass coverslips. Experiments were performed 36 h after transduction. When silencing and transduction occurred together in the same experiment, cells were first transduced for 12 h and then transfected with HiPerfect for the remaining 24 h. THP-1 cells were treated with 20 μM TPA for 24 h to induce monocyte differentiation into macrophages; subsequently cells were transduced with WT mitochondrial-targeted aequorin (Ad-mtAEQ) for 24 h in the presence of TPA, and then transfected with control scrambled siRNA or siRNA-BAP1 (siBAP1#1 and siBAP1#5), in 1% FBS media, for an additional 24 h before Ca^{2+} measurements. For cell imaging experiments, cells were seeded onto 24 mm glass coverslips and allowed to grow to 50% confluence before transduction or transfection.

Transfection with the ER-targeted (D1ER) and the mitochondrial-targeted (4mtD3cpv) Ca^{2+} biosensors[23,37] was performed using Lipofectamine LTX&PLUS (Life Technologies, 15338-100). HEK293 cells were cultured for 24 h, transiently transfected using polyethylenimine (PEI), and used in the experiments 24 h after transfection.

HMESO cells stably expressing empty vector, BAP1, or BAP1(C91S) were generated through transient transfection of the respective plasmid DNA vectors using PEI. Cells were selected using 1.5 mg ml^{-1} G418 to obtain monoclonal populations. Colonies were then grown in 0.5 mg ml^{-1} G418 and tested for BAP1 overexpression via western blot.

Western blot. Total cell (fibroblast cell cultures, human mesothelial cells, HEK293, PPM-Mill, Phi, HMESO, Rob, macrophages, as indicated in the figures) lysates were prepared in M-PER (Thermo Scientific, catalogue number 78501) reagent supplemented with proteases and phosphatases inhibitors (2 mM Na_3VO_4, 2 mM NaF, 50 nM okadaic acid, 1 mM PMSF and protease inhibitor cocktail) and 1 mM DTT.

Cleaved caspase-3 levels were analysed in fibroblasts treated with either vehicle or 100 μM H_2O_2, 10 μM C2-ceramide (C2-Cer), 10 μM menadione (Men), 10 μM 5-fluorouracil for 6 h in DMEM supplemented with 0.1% FBS. When indicated, fibroblasts were silenced for 24 h or transduced with adenoviruses for 36 h as described above. Human mesothelial cells were seeded in DMEM supplemented with 20% FBS, followed by transfection with HiPerfect for 24 h, and then treated with 200 μM H_2O_2 for 6 h, or 5 μg cm^{-2} crocidolite for 24 h, in 0.1% FBS medium. THP-1 cells were treated with 20 μM TPA for 48 h to induce monocyte differentiation into macrophages; subsequently cells were transfected, in 1% FBS media, with control scrambled siRNA, siBAP1#1, and siBAP1#5 for 24 h, and then treated with 5 μg cm^{-2} crocidolite asbestos for an additional 24 h.

Protein extracts were quantified using the Bradford assay (Bio-Rad Laboratories); 7 μg of proteins were loaded and separated on NuPAGE Novex 4–12% Bis-Tris Gel (Life Technologies), and electron-transferred to PVDF (polyvinylidene difluoride) or nitrocellulose membrane according to standard procedures.

Antibodies. Primary antibodies used were α-tubulin (4G1) (Santa Cruz Biotechnology, catalogue number sc-58666), BAP1 (C-4) (Santa Cruz Biotechnology, catalogue number sc-28383), BAP1 (D7W7O) (Cell Signaling, catalogue number 13271), BAP1 (H-300) (Santa Cruz Biotechnology, catalogue

number sc-28236), anti-human CD90 (BD Biosciences, catalogue number 561558), Caspase-3 (Cell Signaling, catalogue number 9662), Flag (Sigma-Aldrich, catalogue number F7425), Histone H2A.X (D17A3) (Cell Signaling, catalogue number 7631), anti-phospho-Histone H2A.X (Ser139) (EMD Millipore, catalogue number 05-636), H3 (Cell Signaling, catalogue number 4499), IP3R1 (Novus Biologicals, catalogue number NB120-5908), IP3R3 (BD Biosciences, catalogue number 610312), anti-Lamin B1 (abcam, catalogue number ab16048), c-myc (Bethyl Laboratories, catalogue number A190-105A), Myc-Tag (9B11) (Cell Signaling, catalogue number 2276), PDI (abcam, catalogue number ab31811) anti-VDAC1 (abcam, catalogue number ab15895). Secondary antibodies used were Goat anti-Mouse IgG (H+L) Secondary Antibody, HRP (Thermo Scientific, catalogue number 32430), Goat anti-Rabbit IgG (H+L) Secondary Antibody, HRP (Thermo Scientific, catalogue number 32460), and Mouse TrueBlot ULTRA: Anti-Mouse Ig HRP (Rockland, catalogue number 18-8817-31).

Quantitative PCR. Total RNA was extracted with TRIzol reagent (Invitrogen, catalogue number 15596-018), followed by phenol/chloroform extractions and ethanol precipitations. The RNA was treated with DNase (Promega) and its integrity and concentration assessed using an Agilent 2100 BioAnalyzer. Complementary DNA was synthesized using a High-Capacity cDNA Reverse Transcription Kit (Invitrogen, catalogue number 4368814) following the manufacturer's instructions. qPCR was performed in triplicate using TaqMan Universal Master Mix II (Invitrogen, catalogue number 4440040) and commercially available TaqMan Probes (Invitrogen) on a StepOnePlus system (Applied Biosystem). The mRNA levels were normalized using the geometric mean of three reference genes (*B2M*, *18S*, and *ACTB*).

Flow cytometry. For cell cycle analyses, fibroblast cell cultures were incubated with 10 μM bromodeoxyuridine (BrdU) for 3.5 h at 37 °C. Cells were collected by trypsinization, fixed, and permeabilized. Cell cycle positions were determined after staining BrdU with FITC (fluorescein isothiocyanate)-labelled anti-BrdU antibody and DNA with 7-ADD using the FITC BrdU Flow Kit (BD Biosciences, catalogue number 559619) according to the manufacturer's instructions. Cells not treated with BrdU, but incubated with FITC anti-BrdU antibody, were used to assess non-specific binding of the anti-BrdU antibody and to set the S-phase gate appropriately.

Cell death was measured in fibroblast cell cultures treated with vehicle or 100 μM H_2O_2 for 6 h, in DMEM supplemented with 0.1% FBS media. Cells were collected and stained with FITC-labelled anti-annexin V and propidium iodide using an FITC Annexin V Apoptosis Detection Kit I (BD Biosciences, catalogue number 556547) according to the manufacturer's instructions. The percentage of late apoptotic cells was determined on the basis of the percentage of cells that were double-positive for both annexin V and propidium iodide (annexin V^+/PI^+).

Primary human mesothelial cells treated with glass or crocidolite asbestos were collected and incubated (blocked) for 20 min with 1% BSA/PBS at 4 °C. Cells were stained with anti-human CD90 PE-Cy7 (BD Biosciences, catalogue number 561558) for 30 min at 4 °C. Cells were washed once with binding buffer and then stained with FITC annexin V and propidium iodide using an FITC Annexin V Apoptosis Detection Kit I (BD Biosciences, catalogue number 556547). After gating on $CD90^+$ cells, the percentages of live cells (annexin V^-/PI^-), early apoptotic cells (annexin V^+/PI^-), and late apoptotic cells (annexin V^+/PI^+) were determined.

For annexin V/propidium iodide experiments, compensation was performed using unstained and single-stained cells, and positivity gates were established using the fluorescence minus one technique.

For all flow cytometry experiments, fluorescence was detected using a BD LSRFortessa flow cytometer (BD Biosciences) and data were analysed using FACSDiva software version 6.2 (BD Biosciences). The investigator was blinded to the genotype and experimental conditions of the samples while conducting the experiments and assessing the outcome.

Immunofluorescence. Cells (fibroblast cell cultures or human mesothelial cells, as indicated in the figures) grown on 24-mm glass coverslips were fixed in 4% paraformaldehyde in PBS for 10 min and washed three times with PBS. Then, cells were permeabilized for 10 min with 0.1% Triton X-100 in PBS and blocked in PBS containing 2% BSA and 0.05% Triton X-100 for 1 h. Cells were incubated overnight at 4 °C with the indicated antibodies: BAP1 (C-4) (1:50), BAP1 (D7W7O) (1:50), BAP1 (H-300) (1:50), PDI (1:50), IP3R3 (1:50), Myc-Tag (1:75), or H3 (1:75). The appropriate isotype-matched, Alexa Fluor-conjugated secondary antibodies (Life Technologies, A11008 (633 goat anti-rabbit, 1:1,000), A-11010 (546 goat anti-rabbit, 1:1,000), and A11001 (488 goat anti-mouse, 1:1,000)) were used. Where indicated, cells were also loaded with 300 nM DAPI (Life Technologies) for 10 min. The coverslips were mounted with ProLong Gold Antifade reagent (Life Technologies), and the analysis of immunofluorescence was performed with a Zeiss LSM 510 confocal laser scanner microscope (Carl Zeiss, Gottingen, Germany) equipped with a 63× oil objective (numerical aperture 1.4) and ZEN lite 2.0 software, or with a Nikon SweptField confocal equipped with a CFI Plan Apo VC60XH objective (numerical aperture 1.4) (Nikon Instruments, Melville, New York, USA) and an Andor DU885 EM-CCD (charge-coupled device) camera (Andor Technology, Belfast, Northern Ireland, UK), or with an Olympus xcellence multiple wavelength high-resolution fluorescence microscopy system equipped with a 60× UPLSAPO objective, numerical aperture 1.35 (Olympus).

Subcellular fractionation. Cell fractionation was performed as previously described[38]. Briefly, 10^9 cells (fibroblast cell cultures, human mesothelial cells, PPM-Mill, HEK293, as indicated in the figure panels) were harvested in PBS and washed by centrifugation at 500*g* for 5 min with PBS. The cell pellet was suspended in homogenization buffer (225 mM mannitol, 75 mM sucrose, 30 mM Tris-HCl pH 7.4, 0.1 mM ethylene glycol-bis(β-aminoethylether)-*N*,*N*,*N*′,*N*′-tetraacetic acid (EGTA), and PMSF (phenylmethylsulfonyl fluoride)) and gently disrupted by Dounce homogenization. The homogenate was centrifuged twice at 600*g* for 5 min to remove nuclei and unbroken cells, and the resultant supernatant was centrifuged at 10,300*g* for 10 min to pellet crude mitochondria. The supernatant was again centrifuged at 20,000*g* for 30 min. Further centrifugation of the supernatant at 100,000*g* for 90 min (70-Ti rotor; Beckman) resulted in the isolation of ER (pellet) and cytosolic fraction (supernatant).

To purify mitochondria, the crude mitochondrial fraction was suspended in isolation buffer (250 mM mannitol, 5 mM HEPES pH 7.4, and 0.5 mM EGTA) and subjected to Percoll gradient centrifugation (Percoll medium: 225 mM mannitol, 25 mM HEPES pH 7.4, 1 mM EGTA, and 30% v/v Percoll) in a 10 ml polycarbonate ultracentrifuge tube, at 95,000*g* for 30 min (SW40 rotor; Beckman). Purified mitochondria were then washed by centrifugation at 6,300*g* for 10 min to remove the Percoll and finally suspended in isolation medium. All centrifugation steps were performed at 4 °C.

To isolate nuclei, cells were collected by centrifugation at 200*g* for 5 min, washed once with ice-cold PBS, suspended in hypotonic buffer (10 mM HEPES pH 7.4, 10 mM KCl, 0.1 mM EDTA, 0.1 mM EGTA, 1 mM DTT, 0.5 mM PMSF), and incubated 15 min on ice. NP40 (Fluka) was added to a final concentration of 0.5% and the mixture was homogenized with a pestle grinder using 30 strokes. The efficiency of shearing the cytoplasm from the nuclei was monitored under a light microscope by staining with Trypan blue. Homogenates were centrifuged at 14,000*g* for 30 s to sediment the nuclei. Nuclei were washed once in PBS and further centrifuged at 14,000*g* for 1 min. Nuclei were finally suspended in hypotonic buffer (20 mM HEPES pH 7.4, 400 mM NaCl, 1 mM EDTA, 1 mM EGTA, 1 mM DTT, 1 mM PMSF), incubated on ice for 30 min, vortexed every 5 min, and centrifuged at 16,000*g* for 10 min; the supernatant was collected as nuclear homogenate.

Immunoelectron microscopy. Fibroblast cell cultures were fixed with 2% paraformaldehyde, 0.2% glutaraldehyde in 0.1 M phosphate buffer pH 7.4 for 1 h at room temperature. Samples were washed in PBS, embedded in 12% gelatin, infiltrated in 2.3 M sucrose, and frozen in liquid nitrogen. Ultrathin cryo-sections were obtained using a Leica EM FC7 cryo-ultramicrotome and collected on copper-formvar-carbon-coated grids. BAP1 localization was revealed using BAP1 (D7W7O) rabbit monoclonal anti-BAP1 antibody (Cell Signaling, catalogue number 13271) and conjugated 10 nm protein A-gold according to published protocols[39]. Sections were imaged with a Zeiss LEO 512 electron microscope and images were acquired by a 2k × 2k bottom-mounted slow-scan Proscan camera controlled by the EsivisionPro 3.2 software.

Intracellular Ca^{2+} concentration measurements. Cytosolic and mitochondrial Ca^{2+} concentration measurements with aequorins. Cells (fibroblast cell cultures, human mesothelial cells, MAF, Phi, HMESO, macrophages, as indicated in the figures) grown on 13-mm round glass coverslips were transduced (or co-transduced in BAP1 gene expression experiments) with aequorin encoded by an adenoviral construct (cytosolic aequorin, cytAEQ; mitochondria-targeted aequorin, mtAEQ; or the low-affinity mitochondrial aequorin, mtAEQmut). The coverslip with the cells was incubated with 5 μM coelenterazine for 2–3 h in 0.1% FBS medium, and then transferred to the perfusion chamber. All aequorin measurements were performed in Krebs-Ringer buffer (135 mM NaCl, 5 mM KCl, 1 mM $MgSO_4$, 0.4 mM KH_2PO_4, 5.5 mM glucose, 20 mM HEPES, pH 7.4) supplemented with 1 mM $CaCl_2$. Agonists and other drugs were added to the same medium, as specified in the text. The experiments were terminated by lysing the cells with 100 μM digitonin in a hypotonic Ca^{2+}-rich solution (10 mM $CaCl_2$ in H_2O), thus discharging the remaining aequorin pool. The light signal was collected and calibrated into $[Ca^{2+}]$ values by an algorithm based on the Ca^{2+} response curve of aequorin at physiological conditions of pH, $[Mg^{2+}]$, and ionic strength, as previously described[36]. Ca^{2+} measurements were conducted using a luminometer in cells transduced with aequorin, which is a bio-luminescent Ca^{2+} probe. Note that $[Ca^{2+}]$ was measured only in cells containing aequorin, specifically providing the results only of the transduced cells, and therefore were not influenced by the background not-transduced cells. To ensure that cells transduced with aequorin

also contained BAP1, BAP1(C91S), or BAP1-targeted chimaeras, we used a transduction ratio of 1 (aequorin) to 3 (BAP1).

ER Ca^{2+} concentration measurements with D1ER. Luminal Ca^{2+} dynamics were measured using single-cell Ca^{2+} imaging and the Ca^{2+}-sensitive fluorescence resonance energy transfer (FRET)-based cameleon protein D1ER[23,37]. Fibroblasts were cultured on 24-mm coverslips. When the cells reached 60% confluence, they were transfected with D1ER. After 36 h, cells were imaged on a Zeiss Axiovert 200M microscope with a cooled CCD camera (Photometrics), equipped with a C-apochromat 40× oil objective (numerical aperture 1.2) and controlled by MetaFluor 7.0 software (Universal Imaging). Emission ratio imaging of the cameleon was accomplished by using a 436DF20 excitation filter, a 450 nm dichroic mirror, and two emission filters (475/40 for enhanced cyan fluorescent protein (ECFP) and 535/25 for citrine) controlled by a Lambda 10-2 filter changer (Sutter Instruments). Fluorescence images were background corrected. Exposure times were typically 100–200 ms, and images were collected every 5–15 s. The FRET signal (yellow fluorescent protein (YFP)/CFP) was normalized to the CFP emission intensity, and changes in ER Ca^{2+} were expressed as the ratio of the emissions at 535 and 470 nm. Cells were treated with 1 μM bradykinin or 500 μM H_2O_2 as indicated in the figures, where representative changes in ER [Ca^{2+}] in *BAP1*^{WT} and *BAP1*$^{+/-}$ fibroblasts are expressed as D1ER ratios (YFP/CFP) normalized to initial values.

Cytosolic Ca^{2+} concentration measurements with Fura-2/AM. Dynamic measurements of cytosolic Ca^{2+} response were performed using the fluorescent Ca^{2+} indicator Fura-2/AM (Life Technologies). Fibroblasts were grown on 24-mm coverslips and incubated at 37 °C for 30 min in 1 mM Ca^{2+}/Krebs-Ringer buffer supplemented with 2.5 mM Fura-2/AM, 0.02% Pluronic F-68 (Sigma), 0.1 mM sulfinpyrazone (Sigma). Cells were then washed and supplied with 1 mM Ca^{2+}/Krebs-Ringer buffer. To determine cytosolic Ca^{2+} response, the cells were placed in an open Leyden chamber on a 37 °C thermostated stage and exposed to 340/380 nm wavelength light using the Olympus xcellence multiple wavelength high-resolution fluorescence microscopy system. H_2O_2 was added to the 1 mM Ca^{2+}/Krebs-Ringer buffer, and crocidolite asbestos or glass added at concentrations of 5 μg cm^{-2}. Ca^{2+} release was recorded upon stimulation as indicated in the figures. To determine whether the Ca^{2+} release occurred via the ER or whether it was secondary to the plasma membrane influx, fibroblasts were loaded with fluorescent Ca^{2+} indicator Fura-2/AM for 30 min in Ca^{2+}-free Krebs-Ringer buffer supplemented with 0.1 mM EGTA. Cells were placed in an open Leyden chamber on a 37 °C thermostated stage and exposed to 340/380 wavelength light, as described above. Bradykinin was added to the Krebs-Ringer buffer, and Ca^{2+} release was recorded upon stimulation as indicated in the figures. The fluorescence data collected were expressed as emission ratios at 340/380 nm. In the figures, the kinetic of the cytosolic Ca^{2+} responses after H_2O_2 or bradykinin stimulation is presented as the ratio of fluorescence at 340/380 nm in cells loaded with Fura-2/AM.

Dynamic measurements of cytosolic Ca^{2+} response after irradiation with UVA (irradiated for 5 min with the Olympus xcellence Hg lamp, model MT-ARC-Hg, 150 W, light was filtered with a 340 filter) or UVB (irradiated at 312 nm for 20 min, at a 2 cm fixed distance, with a Spectroline model ENB-280C/F, 220 V, 50 Hz, 0.17 A) were performed using the fluorescent Ca^{2+} indicator Fura-RED (Life Technologies). Fibroblasts grown on 24-mm coverslips were incubated at 37 °C for 60 min in 1 mM Ca^{2+}/Krebs-Ringer buffer supplemented with 2.5 mM Fura-RED, 0.02% Pluronic F-68 (Sigma), 0.1 mM Sulfinpyrazone (Sigma). Cells were then washed and supplied with 1 mM Ca^{2+}/Krebs-Ringer buffer. To determine the cytosolic Ca^{2+} response, the cells were placed in an open Leyden chamber on a 37 °C thermostated stage and exposed to 406/494 nm wavelength light using the Olympus xcellence multiple wavelength high-resolution fluorescence microscopy system. The fluorescence data collected were expressed as emission ratios at 406/494 nm. In the figures, the kinetics of the cytosolic Ca^{2+} responses after ultraviolet irradiation are presented as the ratio of fluorescence at 406/494 nm in cells loaded with Fura-RED. Statistical analyses refer to normalized FRET fluorescence ratio over time after irradiation ($\Sigma(F_{406\,nm}/F_{494\,nm})$).

Single-cell mitochondria Ca^{2+} measurements with 4mtD3cpv. *BAP1*^{WT} and *BAP1*$^{+/-}$ fibroblasts were transfected with the 4mtD3cpv[23,37] plasmid, as described above. When indicated, co-transfection or silencing were also performed, as described above. After 24 h, cells were imaged on a Zeiss Axiovert 100TV microscope with a cooled CCD camera R3 Retiga (Q-Imaging), equipped with a Fluar 40×/1.3 oil objective and controlled by MetaFluor 7.7.2.0 software (Molecular Devices). Emission ratio imaging of the cameleon was accomplished with a 436DF20 excitation filter, a 450 nm dichroic mirror, and two emission filters (475/40 for ECFP and 535/25 for citrine), controlled by a Lambda 10-2 filter changer (Sutter Instruments). Fluorescence images were background corrected. Exposure times were typically 50–100 ms, and images were collected every 1–2 s. Mitochondrial Ca^{2+} uptake was followed over time after stimulation with 1 μM bradykinin or 100 μM H_2O_2, as indicated in the figures. In the figures, representative traces from single experiments are presented as normalized FRET fluorescence ratio intensity. Statistical analyses refer to normalized FRET fluorescence ratio peak intensity after bradykinin stimulation, or Σ(FRET fluorescence ratio) over time after H_2O_2 stimulation.

Co-immunoprecipitation. Cells (fibroblast cell cultures or HEK293, as indicated in the figures) were collected and lysed in buffer containing 30 mM Tris-HCl, at pH 7.5, 50 mM NaCl, 1% NP-40. To map the BAP1 and IP3R3 binding region, HEK293 cells were transiently transfected using polyethylenimine, collected 24 h later, and lysed in 50 mM Tris, at pH 7.5, 150 mM NaCl, glycerol 10%, 1 mM EDTA, 50 mM NaF, and NP-40 0.1%. All the buffers were supplemented with proteases and phosphatase inhibitors. Extracted proteins were pre-cleared by incubating lysates with G-coated Sepharose beads (GE Healthcare) for 1 h at 4 °C, then the supernatant (700 μg, referred to as 'Input') was incubated overnight with IP3R3 antibody at 4 °C; precipitation of the immune complexes was performed with G-coated Sepharose beads for 4 h at 4 °C, according to the manufacturer's instructions. Alternatively, the supernatant was incubated for 3 h at 4 °C with Flag M2 resin (Sigma, catalogue number A2220) or HA resin (Roche, catalogue number 11815016001). After immunoprecipitation, the beads were washed three times with lysis buffer, at 4 °C, and suspended in 40 μl of 2× Laemmli buffer. Ten to twenty microlitres (depending on experiment) were loaded on the gel and the samples were processed by SDS–polyacrylamide gel electrophoresis (SDS–PAGE) and analysed by western blot.

Duolink proximity ligation *in situ* assay. *BAP1*^{WT} and *BAP1*$^{+/-}$ fibroblasts were fixed in 4% paraformaldehyde for 10 min at 37 °C, and then washed in PBS. Cells were permeabilized with 0.05% Triton X-100 (v/v in PBS) for 10 min at 37 °C. Unspecific binding sites were blocked by incubating cells in 2% BSA (w/v in PBS/0.05% Triton) for 1 h at 37 °C. Cells were then incubated overnight at 4 °C with proximity ligation assay oligonucleotide probes conjugated to primary antibodies specific for IP3R3 (BD Biosciences, catalogue number 610312) and BAP1 (Santa Cruz Biotechnology, catalogue number sc-28236), in diluent buffer according to the Duolink In Situ – Probes Maker protocol (Sigma-Aldrich, catalogue number DUO92101). Detection was performed according to the manufacturer's protocol. Briefly, a ligation-ligase solution was added to each sample for 30 min at 37 °C, and then washed twice for 2 min with 1× Duolink In Situ Wash Buffer A. An amplification-polymerase solution was added for 100 min at 37 °C, and then washed twice for 10 min with 1× Duolink In Situ Wash Buffer B. The slides were mounted using Duolink In Situ Mounting Medium with DAPI. Protein–protein interactions appeared as red dots. Images were processed and red dots counted using the Analyze Particles ImageJ software plugin.

***In vitro* ubiquitylation and deubiquitylation assays.** *In vitro* ubiquitylation assays were performed as previously described[40]. Briefly, Flag-tagged IP3R3(NT) was co-transfected with either empty vector, Myc-tagged BAP1, or the catalytic dead mutant BAP1(C91S) into HEK293 cells. Twenty-four hours after transfection, Flag–IP3R3(NT) was immunoprecipitated with anti-Flag M2 agarose beads. The beads were washed three times in lysis buffer and once in PBS. *In vitro* ubiquitylation assays were performed on immunoprecipitated beads in a volume of 50 μl, containing 50 mM Tris-HCl, at pH 7.5, 5 mM $MgCl_2$, 1 μM okadaic acid, 2 mM ATP, and 0.5 mM DTT, 0.1 μM E1 (Boston Biochem), 0.25 μM Ubch3 (Boston Biochem), 0.25 μM Ubch5c (Boston Biochem), and 2.5 μg μl^{-1} human ubiquitin (Boston Biochem). Samples were incubated for 1 h at 33 °C, washed twice with PBS at 4 °C, suspended in 2× Laemmli buffer, and analysed by SDS–PAGE and western blot.

For *in vitro* deubiquitylation assays, HEK293 cells were transfected with Flag–IP3R3(NT), Myc–BAP1, or Myc–BAP1(C91S). Flag–IP3R3(NT) was immunopurified and *in vitro* ubiquitylation was performed. Then, beads were washed twice with PBS at 4 °C, and suspended in deubiquitylation reaction buffer containing 50 mM Tris-HCl, at pH 7.5, 5 mM $MgCl_2$, 1 μM okadaic acid, 2 mM ATP, and 0.5 mM DTT. Myc–BAP1 and Myc–BAP1(C91S) were purified with a c-Myc-tagged Protein Mild Purification Kit version 2 (MBL International, catalogue number 3305), eluted with c-Myc-tag peptide accordingly to the manufacturer's instructions, and added to the deubiquitylation reaction buffer. Samples were incubated at 33 °C for the indicated times, then beads were washed twice with PBS at 4 °C, and suspended in 2× Laemmli buffer. Samples were processed by SDS–PAGE and analysed by western blot.

Neutral comet assay. *BAP1*^{WT} and *BAP1*$^{+/-}$ fibroblasts were plated at 8×10^5 cells per T25 flask and incubated overnight, then the medium was replaced with cold PBS, and cells were irradiated, on ice, with 6 Gy ionizing radiation dose using a cabinet X-ray system (Faxitron). After ionizing radiation, cells were collected immediately (detached using trypsin, harvested, and frozen in 90% FBS/10% DMSO) or incubated in complete growth medium for the indicated time before being collected. Neutral comet assay and data analysis were performed by Trevigen (https://www.trevigen.co). Samples were tested using Trevigen's Comet

Assay Electrophoresis System. Images were captured and analysed using a Loats Associates Comet Analysis System. At least 200 cells were scored per sample. Trevigen Neutral Control Cells were used as electrophoresis controls. Data from triplicate wells for each sample were pooled to calculate the median and mean, and expressed as tail moment. Experiments were conducted and analysed by investigators blinded to the genotype and experimental conditions of the samples.

Kinetics of H2A.X phosphorylation. $BAP1^{WT}$ and $BAP1^{+/-}$ fibroblasts were plated and treated with 6 Gy ionizing radiation, as described for neutral comet assay. In ultraviolet radiation experiments, fibroblasts were plated at 3.5×10^5 cells per 60 mm dish and incubated overnight, then the medium was replaced with PBS and cells were irradiated with 50 mJ cm^{-2} of either UVA (340 nm, using a UVA-340 sunlamp, Atlas Material Testing Technology) or UVB (290–315 nm, using a Philips UVB Broadband TL 40 W/12 RS SLV/25). For UVA and UVB, spectral output was quantified with a General UV-513/AB Digital UV AB Light Meter.

After radiation, cells were collected immediately or incubated in complete growth medium for the indicated time before being collected. Dry cell pellets were immediately store at −80 °C. Samples were boiled at 95 °C for 10 min. Total cell lysates were immediately prepared by sonication in 200 µl of buffer containing 25 mM Tris-HCl pH 7.5 and 1% SDS. After centrifugation, the supernatant was collected and the protein concentration determined using a Pierce BCA Protein Assay Kit (Life Technologies, catalogue number 23225). SDS–PAGE and western blot were conducted according to standard procedure (see above).

Clonogenic survival assay after exposure to ionizing or ultraviolet radiation. In ionizing radiation experiments, $BAP1^{WT}$ and $BAP1^{+/-}$ fibroblasts were plated and treated with the indicated ionizing radiation, as described for the neutral comet assay. In ultraviolet radiation experiments, fibroblasts were plated at 3.5×10^5 cells per 60 mm dish and incubated overnight, then the medium was replaced with PBS and the cells were irradiated with 25 mJ cm^{-2} as described above in the section Kinetics of H2A.X phosphorylation.

After irradiation, fibroblasts were trypsinized, harvested, counted, and plated on six-well plates. Cells were incubated at 37 °C for 14 days (the tissue culture medium was changed twice a week) to allow colony formation. The surviving colonies were washed with PBS and fixed and stained with 0.5% crystal violet in 50/50 methanol/water for 10 min, followed by three washes with PBS. Colonies were counted and the plating efficiencies were calculated for untreated cells as the ratio of the number of colonies to the number of cells seeded. The surviving fractions, expressed in terms of plating efficiency, were calculated as the ratio between the number of colonies arising after treatment and the number of cells seeded × plating efficiency.

***In vitro* cell transformation assay.** The human mesothelial cell transformation assay was done according to an established protocol[28,41]. Human mesothelial cells were cultured and seeded in six-well plates at a density of 3×10^5 cells per well in 20% FBS growth medium. After 24 h, the medium was switched to 0.1% FBS, and transfection performed with HiPerfect as described above. When indicated, transduction of cells was performed 6 h after HiPerfect transfection. Twenty-four hours later, human mesothelial cells were pre-treated with 10 ng ml^{-1} recombinant human TNFα (PromoKine, catalogue number C-63720) or 0.1% BSA (vehicle), and incubated for an additional 24 h. At this time point, human mesothelial cells were exposed to 5 µg cm^{-2} crocidolite asbestos fibres or PBS (control) for 48 h. Human mesothelial cells were then maintained in 10% FBS supplemented with 10 ng ml^{-1} TNFα. Transfection transduction was repeated every 96 h in fresh 10% FBS supplemented with 10 ng ml^{-1} TNFα. Media were completely replaced 24 h after transfection transduction, then cells were incubated at 37 °C for the remaining 72 h. After 2–3 weeks, three-dimensional foci were identified and counted under a light microscope. Experiments were performed three times.

Statistics and reproducibility. Statistical analyses were performed using Student's two-tailed unpaired *t*-tests, unless otherwise specified. *P* values <0.05 were considered statistically significant and marked with asterisks ($*P<0.05$; $**P<0.01$; $***P<0.001$), as indicated in the figure legends. All data collected met the normal distributions assumption of the test. Data are represented as mean ± s.e.m., unless otherwise specified. The exact sample size (*n*) for experimental groups/conditions, and whether samples represent technical or cell culture replicates, are indicated in the figure legends and Supplementary Tables. The exact sample sizes of Ca^{2+} experiments are reported in Supplementary Tables 1 and 2. For all other experiments, unless otherwise specified, the results shown are representative of experiments independently conducted three times that produced similar results.

Data availability. The authors declare that the data supporting the findings of this study are either available within the paper (and its Supplementary Information files) or are available from the corresponding authors upon reasonable request.

31. Vangipuram, M., Ting, D., Kim, S., Diaz, R. & Schüle, B. Skin punch biopsy explant culture for derivation of primary human fibroblasts. *J. Vis. Exp.* **77,** e3779 (2013).
32. Bocchetta, M. *et al.* Human mesothelial cells are unusually susceptible to simian virus 40-mediated transformation and asbestos cocarcinogenicity. *Proc. Natl Acad. Sci. USA* **97,** 10214–10219 (2000).
33. Pass, H. I. *et al.* Characteristics of nine newly derived mesothelioma cell lines. *Ann. Thorac. Surg.* **59,** 835–844 (1995).
34. Tsuchiya, S. *et al.* Induction of maturation in cultured human monocytic leukemia cells by a phorbol diester. *Cancer Res.* **42,** 1530–1536 (1982).
35. Dey, A. *et al.* Loss of the tumor suppressor BAP1 causes myeloid transformation. *Science* **337,** 1541–1546 (2012).
36. Bonora, M. *et al.* Subcellular calcium measurements in mammalian cells using jellyfish photoprotein aequorin-based probes. *Nat. Protocols* **8,** 2105–2118 (2013).
37. Palmer, A. E. & Tsien, R. Y. Measuring calcium signaling using genetically targetable fluorescent indicators. *Nat. Protocols* **1,** 1057–1065 (2006).
38. Wieckowski, M. R., Giorgi, C., Lebiedzinska, M., Duszynski, J. & Pinton, P. Isolation of mitochondria-associated membranes and mitochondria from animal tissues and cells. *Nat. Protocols* **4,** 1582–1590 (2009).
39. Slot, J. W. & Geuze, H. J. Cryosectioning and immunolabeling. *Nat. Protocols* **2,** 2480–2491 (2007).
40. Kuchay, S. *et al.* FBXL2- and PTPL1-mediated degradation of p110-free p85β regulatory subunit controls the PI(3)K signalling cascade. *Nat. Cell Biol.* **15,** 472–480 (2013).
41. Yang, H. *et al.* Programmed necrosis induced by asbestos in human mesothelial cells causes high-mobility group box 1 protein release and resultant inflammation. *Proc. Natl Acad. Sci. USA* **107,** 12611–12616 (2010).

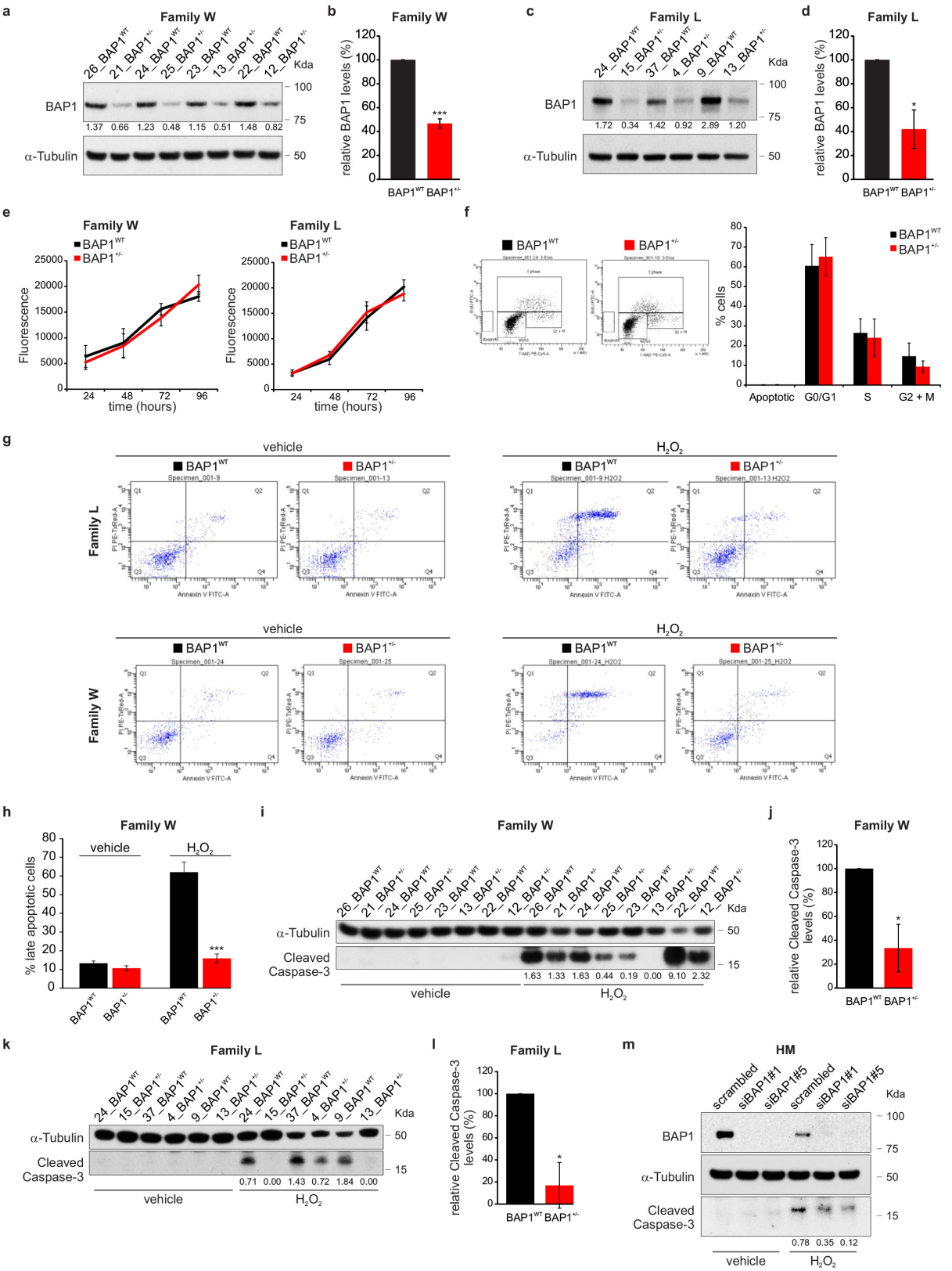

Extended Data Figure 1 | See next page for caption.

Extended Data Figure 1 | Fibroblasts from *BAP1* germline mutation carriers have reduced BAP1 protein levels, do not show differences in growth or cell cycle progression, and are protected from apoptosis. **a**–**d**, Western blot: amounts of wild-type BAP1 in total cell lysates of W (**a**) and L (**c**) fibroblasts, matched by gender and age (see Supplementary Fig. 1; that is, W: 26_BAP1^{WT} and 21_BAP1$^{+/-}$; and so on, as shown in subsequent figures); decimals indicate the amounts of BAP1 relative to α-tubulin as per densitometry. **b**, **d**, Densitometric analyses. BAP1 protein levels normalized to α-tubulin in fibroblast cell cultures from W (**b**) and L (**d**) family members matched by gender and age; data shown as mean ± s.e.m. of $n = 4$ (**b**) and $n = 3$ (**d**) biological replicates per condition, representative of three or more independent experiments. **e**, AlamarBlue assay was used to measure cell growth at the indicated time points, in fibroblasts from W (left) and L (right) family members; data shown as mean ± s.d. of $n = 6$ technical replicates per data point, representative of three or more independent experiments in biological replicates. **f**, Flow cytometry analyses showing percentage of cells in different phases of the cell cycle; data shown as mean ± s.e.m. of $n = 4$ biological replicates per condition. No differences were observed between *BAP1*^{WT} and *BAP1*$^{+/-}$ fibroblasts from either W or L family members. **g**, Representative flow cytometry dot plots assessing annexin V/FITC and propidium iodide staining in fibroblasts from L (upper panels, $n = 4$ independent experiments: three biological replicates per condition, one culture replicate) and W (lower panels, $n = 4$ biological replicates per condition) family members treated with 100 μM H_2O_2 for 6 h. **h**, Late apoptotic cells calculated as the percentage of gated cells in the top right quadrant (Q2: annexin V$^+$/PI$^+$); data shown as mean ± s.e.m. of $n = 4$ biological replicates per condition. **i**–**l**, Cleaved caspase-3 levels measured by western blot in fibroblast cell cultures from W (**i**) and L (**k**) family members, matched by gender and age, treated with H_2O_2. Decimals indicate the densitometrically determined amounts of cleaved caspase-3 relative to α-tubulin. **j**, **l**, Cleaved caspase-3 densitometry of bands in *BAP1*$^{+/-}$ fibroblasts expressed relatively to the amounts detected in *BAP1*^{WT} fibroblasts (100%); data shown as mean ± s.e.m. of $n = 4$ (**j**) and $n = 3$ (**l**) biological replicates per condition, representative of at least three independent experiments. **m**, Primary human mesothelial cells were transfected with control scrambled siRNA, or siRNAs–BAP1 (siBAP1#1 and siBAP1#5). After 24 h, cells were treated with 200 μM H_2O_2 for 6 h. Total cell lysates were prepared and analysed by western blot to compare cleaved caspase-3 levels. Decimals indicate densitometrically determined cleaved caspase-3 levels normalized to α-tubulin. Similar results were obtained in three separate human mesothelial cell primary cultures from different donors. Black, *BAP1*^{WT}; red, *BAP1*$^{+/-}$; $*P < 0.05$; $***P < 0.001$, calculated using two-tailed unpaired Student's *t*-tests. For western blot source images, see Supplementary Fig. 2.

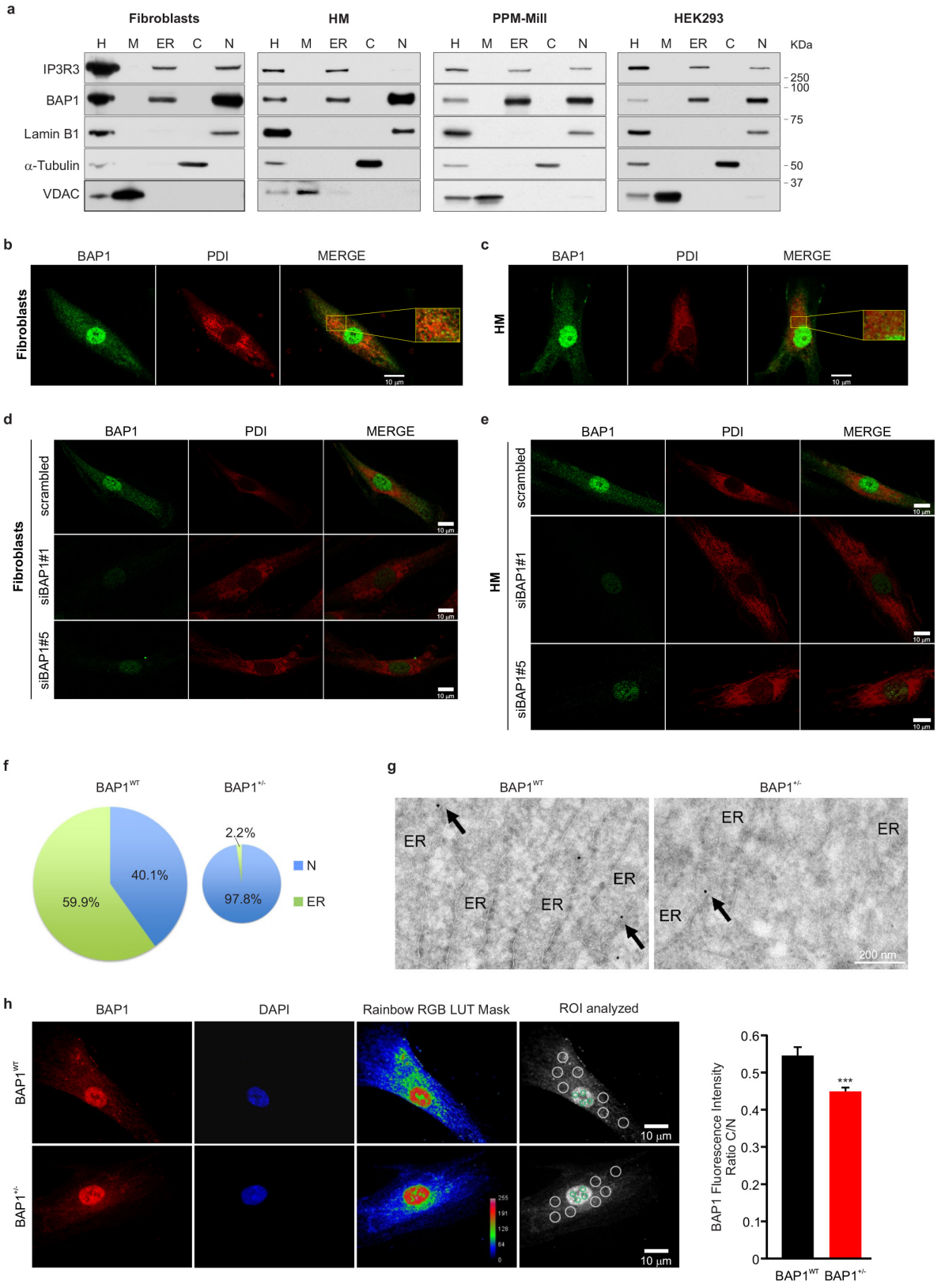

Extended Data Figure 2 | See next page for caption.

Extended Data Figure 2 | Subcellular fractionation and immunofluorescence showing BAP1 localization at the ER. a, Western blot showing the amounts of BAP1 in the subcellular fractions of primary fibroblasts, human mesothelial cells, PPM-Mill (a human malignant mesothelioma cell line), and HEK293 (human embryonic kidney cells). H, homogenate; M, mitochondria; C, cytosol; N, nuclei. Markers: mitochondria (VDAC), ER (IP3R3), nuclei (Lamin B1), cytosol (α-tubulin). **b**, **c**, Immunofluorescence: BAP1 localization in WT fibroblasts (**b**) and human mesothelial cells (**c**). Cells were immunostained for BAP1 (green) and PDI (ER marker, red). Merged images show the overlapping yellow signal between BAP1 and PDI. Inserts show magnified merged images. BAP1, besides its nuclear localization, shows a diffuse pattern of punctate hyper-fluorescent spots in the cytoplasm that co-localized with the ER, both in $BAP1^{WT}$ fibroblasts (**b**) and in human mesothelial cells (**c**). Representative immunofluorescence images from $n = 10$ fields of view; scale bar, 10 μm. **d**, **e**, The specificity of BAP1 immunofluorescence staining was confirmed by complete disappearance of this immunofluorescence pattern when BAP1 was downregulated using two different siRNAs, but not in cells transfected with scrambled siRNA. Immunofluorescence in wild-type fibroblasts (**d**) and human mesothelial cells (**e**) after BAP1 silencing. Cells were transfected with control scrambled siRNA or siRNAs–BAP1 (siBAP1#1 and siBAP1#5). After 24 h, the cells were immuno-stained using monoclonal antibodies for BAP1 (green) and PDI (ER marker, red). Merged images show the overlapping signal (yellow) between BAP1 and PDI. Representative immunofluorescence images from $n = 5$ fields of view per condition; scale bar, 10 μm. **f**, Percentages of nuclear (N) and ER-localized BAP1 in $BAP1^{WT}$ and $BAP1^{+/-}$ fibroblasts, related to Fig. 1d. Densitometric analysis of the intensity of the bands was performed using ImageJ, and the amounts of nuclear and ER-localized BAP1 were normalized on the respective markers, lamin B1 (nuclei) and IP3R1 (ER). The total, combined, amount of nuclear and ER BAP1 was reduced by 47.9% in $BAP1^{+/-}$ fibroblasts, depicted by the smaller size of the pie chart. Percentages of BAP1 in the nuclear or ER fractions are relative to the total amount of nuclear and ER BAP1. **g**, Immunogold BAP1 labelling of cryo-sections in $BAP1^{WT}$ and $BAP1^{+/-}$ fibroblasts. Note reduced detection of BAP1 associated with the ER (arrows) in $BAP1^{+/-}$ cells; scale bar 200 nm. **h**, Immunofluorescence showing reduced cytoplasm/nucleus (C/N) ratio intensity in $BAP1^{+/-}$ fibroblasts. Cells were stained with DAPI (nuclei, blue) and BAP1 (red). Representative images from $n = 20$ fields of view per condition. Rainbow RGB LUT (red, green, blue look-up table) mask shows colour-coded contrast and pseudocolouring according to an arbitrary colour LUT (see pseudocolour scale, numbers on the scale are 0, black; 64, blue; 128, green; 191, light red; 255, darker red). Scale bar, 10 μm. The bar graph shows the mean ± s.e.m. of the cytoplasm/nucleus ratio intensity measured in random regions of interest (ROIs) of the acquired images: the areas (regions of interest) where the intensities of fluorescence were measured are indicated by white and green circles in the cytoplasm and nucleus respectively ($n = 40$ cells for $BAP1^{WT}$; $n = 46$ cells for $BAP1^{+/-}$); $^{***}P < 0.001$. P value calculated using two-tailed unpaired Student's t-test. For western blot and electron microscopy source images, see Supplementary Figs 2 and 3.

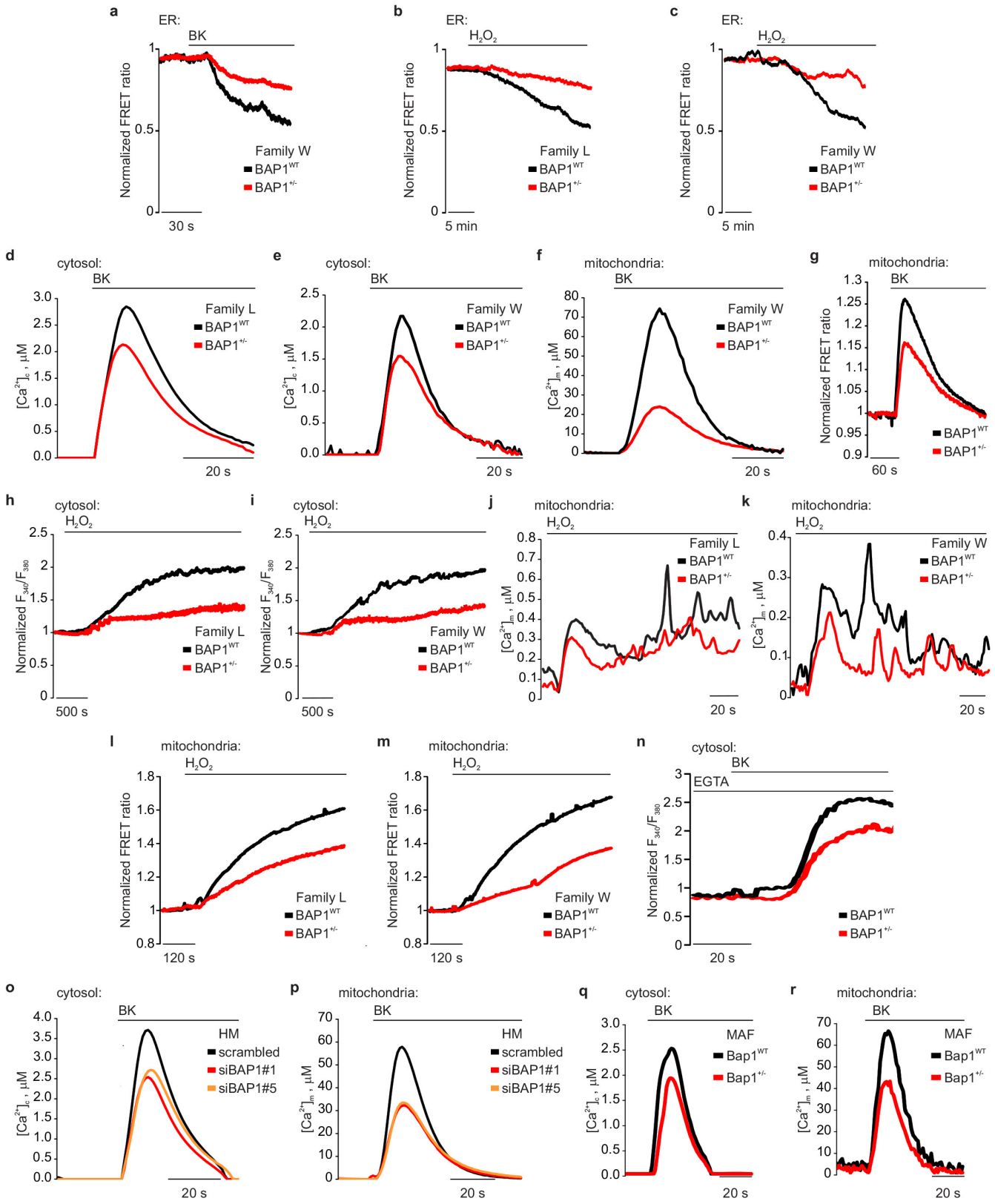

Extended Data Figure 3 | See next page for caption.

Extended Data Figure 3 | BAP1 modulates intracellular Ca^{2+} homeostasis. a, *BAP1*$^{+/-}$ W-fibroblasts displayed reduced Ca^{2+} release from the ER after stimulation with 1 μM bradykinin compared with wild-type fibroblasts (see also Fig. 1e). **b**, **c**, *BAP1*$^{+/-}$ L (**b**) and W (**c**) fibroblasts showed reduced Ca^{2+} release from the ER after stimulation with H_2O_2. **d**, **e**, *BAP1*$^{+/-}$ L (**d**) and W (**e**) fibroblasts had reduced cytosolic Ca^{2+} concentrations ($[Ca^{2+}]_c$) after stimulation with 1 μM bradykinin. **f**, *BAP1*$^{+/-}$ W-fibroblasts, stimulated with 1 μM bradykinin displayed reduced mitochondrial Ca^{2+} concentrations ($[Ca^{2+}]_m$) (see also Fig. 1f). **g**, Representative traces of single-cell Ca^{2+} measurements using mitochondrial-targeted cameleon (4mtD3cpv) showing reduced mitochondrial Ca^{2+} in *BAP1*$^{+/-}$ fibroblasts upon treatment with 1 μM bradykinin. **h**, **i**, *BAP1*$^{+/-}$ L (**h**) and W (**i**) fibroblasts showed reduced cytosolic Ca^{2+} after stimulation with H_2O_2. **j**, **k**, *BAP1*$^{+/-}$ L (**j**) and W (**k**) fibroblasts displayed reduced $[Ca^{2+}]_m$ after stimulation with H_2O_2. **l**, **m**, Representative time-lapse traces of single-cell Ca^{2+} measurements using 4mtD3cpv showing reduced mitochondrial Ca^{2+} in *BAP1*$^{+/-}$ L (**l**) and W (**m**) fibroblasts after stimulation with 100 μM H_2O_2 for 20 min. **n**, Reduced intracellular Ca^{2+} levels in stimulated *BAP1*$^{+/-}$ fibroblasts are independent of extracellular Ca^{2+} influx from the plasma membrane. *BAP1*$^{+/-}$ and matched wild-type fibroblasts were loaded with Fura-2/AM in Ca^{2+}-free Krebs-Ringer buffer supplemented with 0.1 mM EGTA, then dynamic measurements of intracellular Ca^{2+} levels were conducted after addition of 1 μM bradykinin to the same buffer. Changes in intracellular Ca^{2+} responses after bradykinin stimulation are displayed as the ratio of fluorescence at 340/380 nm. **o**, **p**, Human mesothelial cells silenced for BAP1 displayed reduced $[Ca^{2+}]_c$ (**o**) and $[Ca^{2+}]_m$ (**p**) after stimulation with 1 μM bradykinin. Human mesothelial cell cultures were transfected with control scrambled siRNA or siRNAs–BAP1 (siBAP1#1 and siBAP1#5). After 24 h, cells were stimulated with 1 μM bradykinin and $[Ca^{2+}]_c$ (**o**) and $[Ca^{2+}]_m$ (**p**) were measured using targeted aequorin probes. **q**, **r**, MAFs derived from *Bap1*$^{+/-}$ mice displayed reduced $[Ca^{2+}]_c$ (**q**) and $[Ca^{2+}]_m$ (**r**) compared with *Bap1*^{WT} mice, and thus they reproduce the human condition. Representative changes in $[Ca^{2+}]_c$ (**q**) and $[Ca^{2+}]_m$ (**r**) in MAF cells after agonist stimulation (100 μM bradykinin). For source data, see Supplementary Tables 1 and 2.

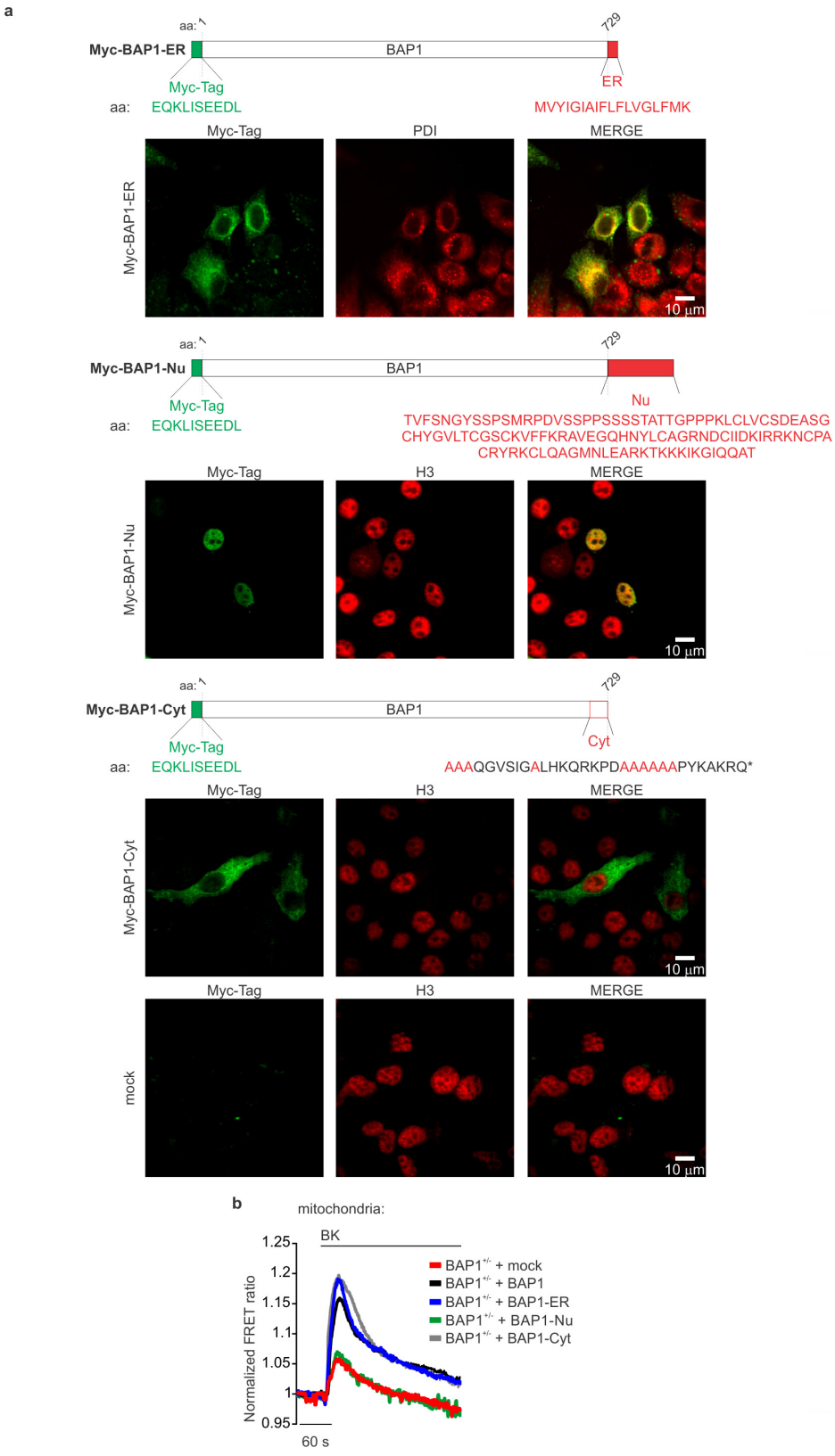

Extended Data Figure 4 | See next page for caption.

Extended Data Figure 4 | BAP1 targeting to ER, nucleus, and cytoplasm differentially affects mitochondrial Ca^{2+} homeostasis. a, Localization of Myc-tagged BAP1 chimaeras. Immunofluorescence: BAP1 localization in wild-type fibroblasts. ER chimaera (Myc–BAP1-ER): BAP1 was fused to the ER targeting sequence from the yeast UBC6 protein to target BAP1 to the cytosolic face of the ER membrane. Nuclear chimaera (Myc–BAP1-Nu): BAP1 was fused to a sequence derived from the glucocorticoid receptor NR3C1. Cytoplasmic chimaera (Myc–BAP1-Cyt): point mutations were introduced in the NLS region of BAP1 to prevent its nuclear localization (*stop codon). BAP1 localization is shown in green using a Myc-Tag antibody; the nuclei and the ER are shown in red using histone H3 (nucleus) and PDI (ER) antibodies. The merged signal is shown in yellow. Note the specific localization of the three chimaeras to the ER, nuclei, and cytoplasm. Mock, empty vector (control). Representative immunofluorescence images from $n = 5$ fields of view per condition; scale bar, 10 μm. **b**, Representative traces of single-cell Ca^{2+} measurements in $BAP1^{+/-}$ fibroblasts co-transfected with mitochondrial-targeted 4mtD3cpv and either BAP1 or targeted BAP1-ER, BAP1-Nu, BAP1-Cyt; mock, co-transfection with an empty vector. Mitochondrial Ca^{2+} uptake was followed over time after stimulation with 1 μM bradykinin. Descriptive statistics are shown in Supplementary Table 1.

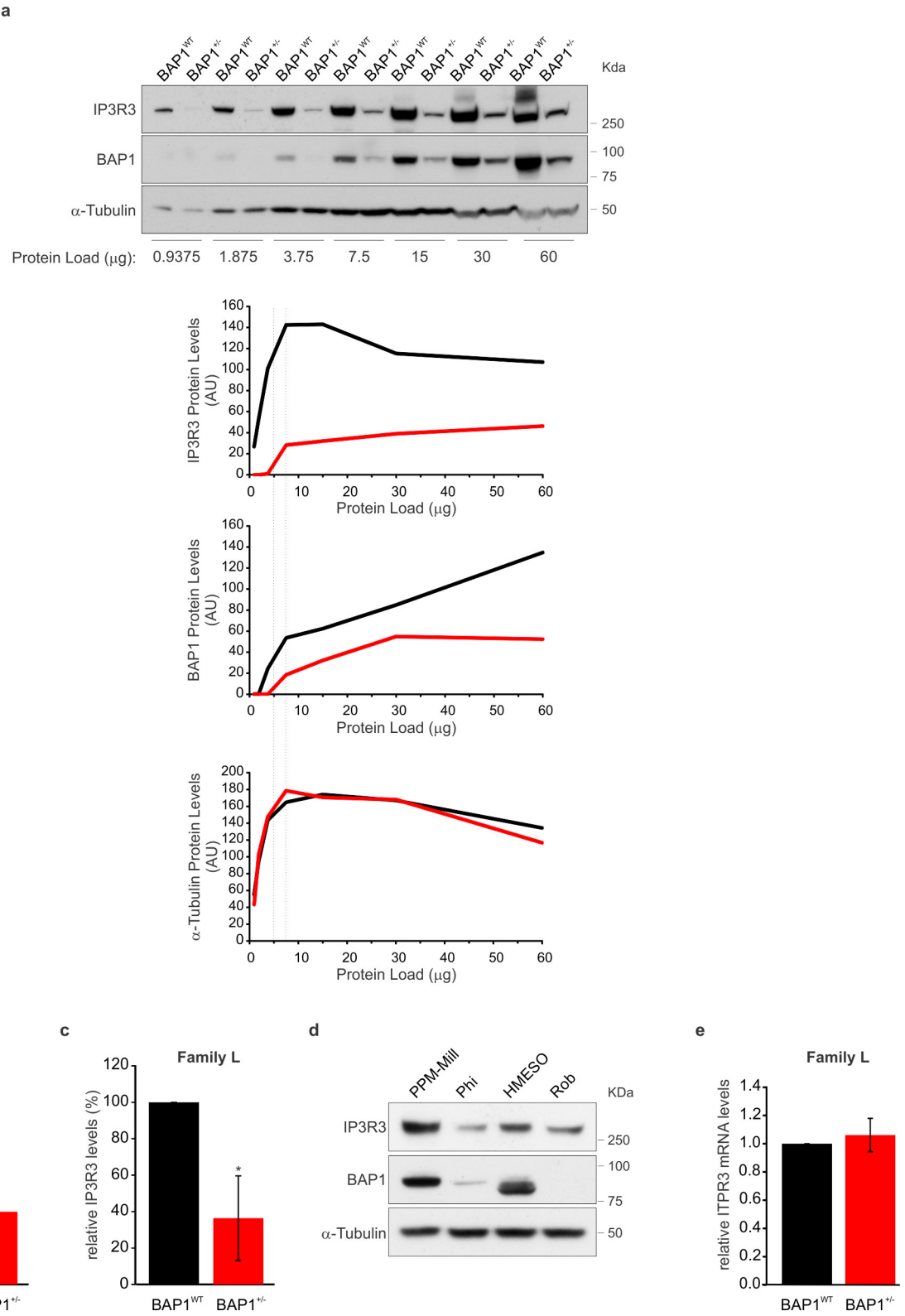

Extended Data Figure 5 | See next page for caption.

Extended Data Figure 5 | BAP1 stabilizes IP3R3. a, Defining the linear dynamic range of BAP1 and IP3R3 detection by western blot. The top panel shows a representative western blot performed on a twofold dilution series (from 60 to 0.9375 μg) of total cell homogenates from $BAP1^{+/-}$ and matched control $BAP1^{WT}$ fibroblasts. Protein levels were determined using the following primary antibodies: BAP1 (C-4), Santa Cruz Biotechnology, catalogue number sc-28383, 1:300; IP3R3, BD Biosciences, catalogue number 610312, 1:500; α-tubulin (4G1), Santa Cruz Biotechnology, catalogue number sc-58666, 1:15,000. A horseradish peroxidase-conjugated secondary antibody (Stabilized Peroxidase Conjugated Goat Anti-Mouse, Thermo Scientific, catalogue number 32430; 1:1,000 for BAP1 and IP3R3, 1:5,000 for α-tubulin) was used to generate the chemiluminescent signal captured on autoradiography film. Digital images were acquired, then densitometric analysis of the intensity of the bands was performed using ImageJ, and expressed as arbitrary optical densitometry units (AU). The lower three panels show the arbitrary optical densitometry units for IP3R3, BAP1, and α-tubulin, plotted against the protein load. The dotted lines define the linear dynamic range of protein load for BAP1, IP3R3, and α-tubulin detection. **b**, **c**, Densitometric analysis of IP3R3 protein levels normalized to α-tubulin in fibroblasts from W (**b**) and L (**c**) family members, related to Fig. 2A, B. Densitometry of bands in $BAP1^{+/-}$ fibroblasts is expressed relative to $BAP1^{WT}$ fibroblasts (100%), matched by gender and age as indicated in Supplementary Fig. 1a, b; data shown as mean ± s.e.m. of $n = 4$ (**b**) and $n = 3$ (**c**) biological replicates per condition, representative of three independent experiments; $^{*}P < 0.05$ calculated using two-tailed paired Student's *t*-tests. **d**, Malignant mesothelioma cell lines with mutated BAP1 contained reduced amounts of IP3R3: PPM-Mill (wild-type BAP1), Phi (mutated BAP1 with shorter splicing isoform), HMESO (mutated BAP1 alternative splicing, shorter protein), and Rob (BAP1 null). **e**, Quantitative PCR analysis of *ITPR3*, the gene that codes for IP3R3. mRNA expression levels were normalized using the geometrical mean of *B2M*, *18S*, and *ACTB* reference genes in $BAP1^{WT}$ and $BAP1^{+/-}$ fibroblasts. mRNA expression levels in $BAP1^{+/-}$ fibroblasts are expressed relative to $BAP1^{WT}$. Data shown as mean ± s.e.m. of $n = 6$ technical replicates, representative of three independent experiments in biological replicates. For western blot source images, see Supplementary Fig. 2.

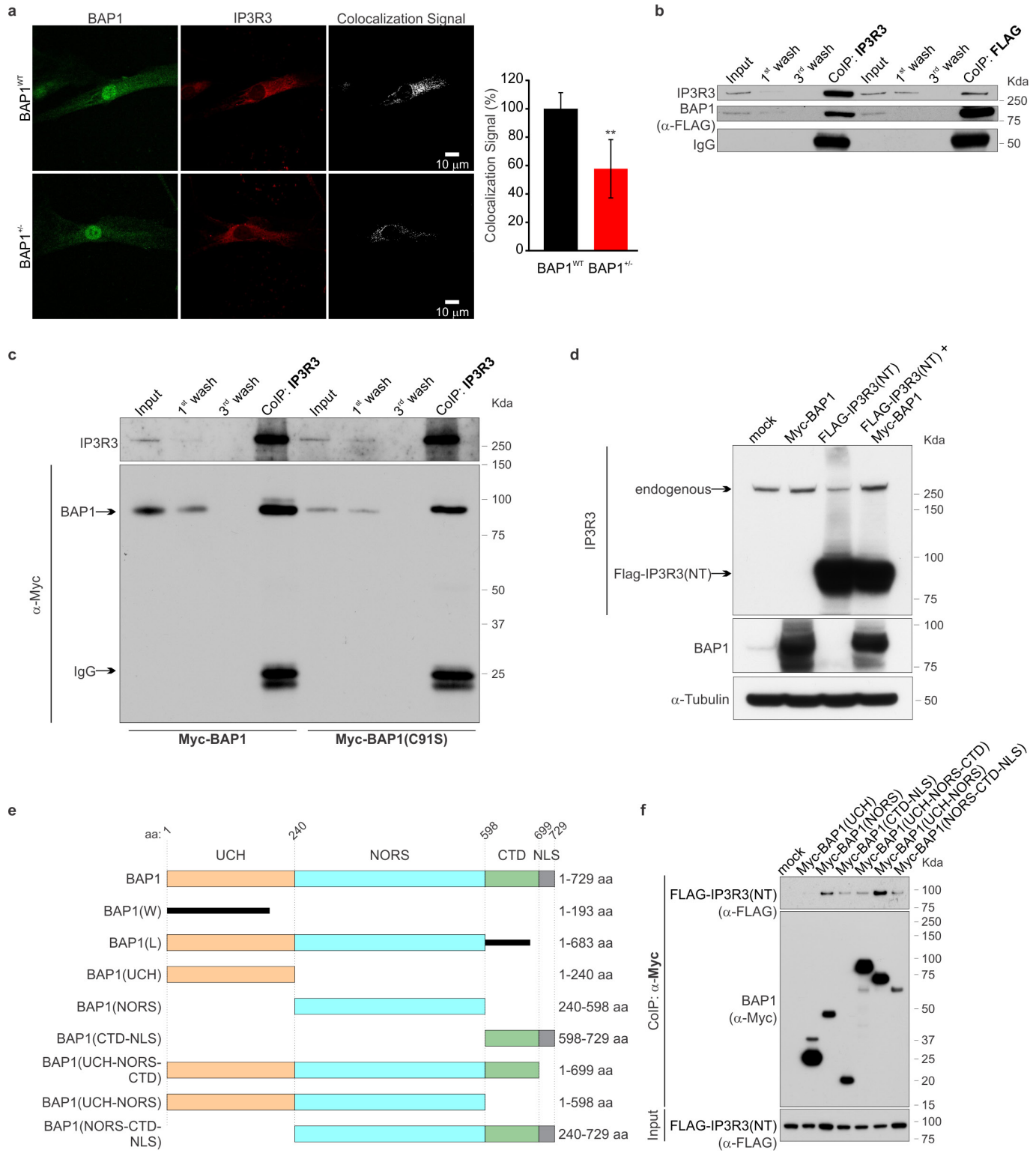

Extended Data Figure 6 | See next page for caption.

Extended Data Figure 6 | BAP1 binds IP3R3. a, Immunofluorescence, reduced BAP1 colocalization with IP3R3 in $BAP1^{+/-}$ fibroblasts compared with $BAP1^{WT}$ fibroblasts. Cells were immunostained for BAP1 (green) and IP3R3 (red). Images were processed with ImageJ software equipped with the Colocalization Highlighter plugin; the colocalization signal is shown in white. Scale bar, 10 μm. The bar graph depicts the decreased colocalization of BAP1 and IP3R3 in $BAP1^{+/-}$ fibroblasts, expressed as (%) mean ± s.e.m.; $^{**}P < 0.01$ ($n = 9$ cells per condition), P value calculated using two-tailed unpaired Student's t-tests. **b**, Co-immunoprecipitation (CoIP) of IP3R3 and BAP1 from HEK293 cells stably expressing Flag–HA–BAP1. **c**, Co-immunoprecipitation of endogenous IP3R3 and Myc-tagged wild-type BAP1 or the catalytically inactive BAP1(C91S). Washes (first and third) show loss of bound proteins that washed out during three sequential washes of the immuno-complexes. BAP1(C91S) retains the ability to bind IP3R3. **d**, The dominant negative effect of NT-IP3R3 overexpression on endogenous IP3R3 levels is counteracted by concomitant BAP1 overexpression, findings indicating that BAP1 binds IP3R3 and prevents its degradation. **e**, Schematic representation of BAP1 domains, truncated W and L mutants (see also ref. 5), and fragments. Domains of the 729-amino-acid BAP1 protein (1–729 amino acids), consisting of an N-terminal UCH domain (1–240 amino acids), a non-regular secondary structure (NORS) domain (240–598 amino acids), a C-terminal (CTD) domain (598–699 amino acids), and NLS (699–729). Numbers refer to amino-acid positions. BAP1(W) and BAP1(L) are the predicted truncations of BAP1 resulting from the germline mutations in W and L families, respectively. **f**, Mapping of the BAP1 region interacting with IP3R3. HEK293 cells were co-transfected with Flag–IP3R3(NT) and the indicated Myc-tagged BAP1 fragments expression vectors; cell extracts were used for co-immunoprecipitation with anti-Myc resin. The BAP1 region UCH–NORS had the highest binding affinity to Flag–IP3R3(NT), and the CTD–NLS region contributed to the binding, while the UCH region alone showed no interaction. For western blot source images, see Supplementary Fig. 2.

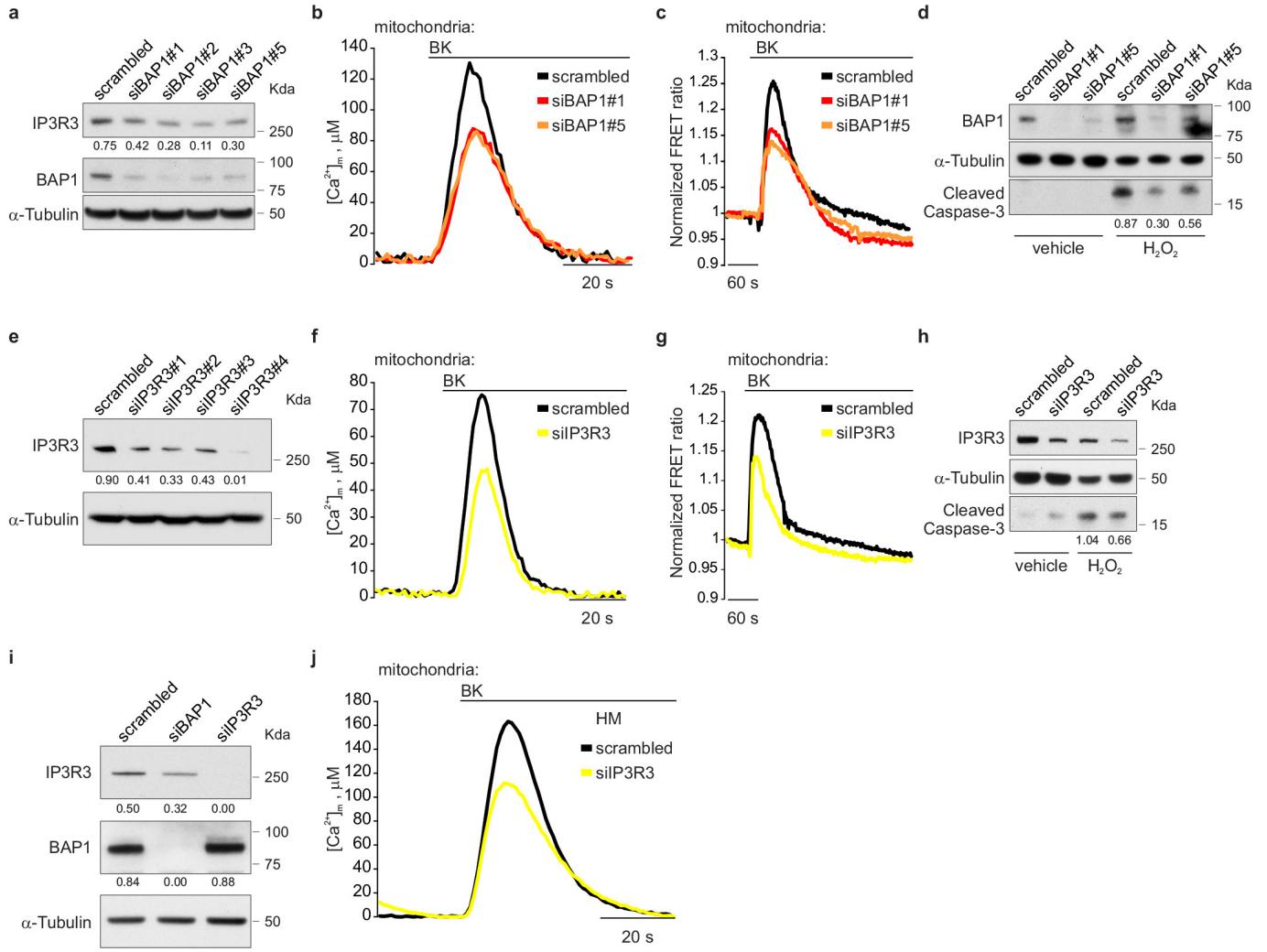

Extended Data Figure 7 | Effects of BAP1 silencing on IP3R3 protein levels, mitochondrial Ca^{2+} uptake, and apoptosis. a, Western blot of BAP1 and IP3R3 protein levels in *BAP1*^{WT} fibroblasts silenced for BAP1. **b**, $[Ca^{2+}]_m$ measurements after stimulation with 1 μM bradykinin in *BAP1*^{WT} fibroblasts transfected with control scrambled siRNA or siRNAs–BAP1 (siBAP1#1 and siBAP1#5). **c**, Representative traces of single-cell Ca^{2+} measurements in *BAP1*^{WT} fibroblasts transfected with mitochondrial-targeted 4mtD3cpv and control scrambled siRNA, or siBAP1#1 and siBAP1#5; mitochondrial Ca^{2+} uptake was followed over time after stimulation with 1 μM bradykinin. **d**, Reduced sensitivity to apoptosis after treatment with 100 μM H_2O_2 for 6 h in *BAP1*^{WT} fibroblasts after BAP1 silencing. **e**–**h**, IP3R3 silencing in *BAP1*^{WT} fibroblasts (**e**) leads to decreased mitochondrial Ca^{2+} uptake after stimulation with 1 μM bradykinin—as shown both by cell-population experiments with mitochondrial-targeted aequorin (**f**) or single-cell experiments with 4mtD3cpv (**g**)—and protection from apoptosis (**h**). **i**, **j**, BAP1 or IP3R3 silencing in primary human mesothelial cells leads to reduced IP3R3 protein levels (**i**), and decreased $[Ca^{2+}]_m$ after stimulation with 1 μM bradykinin (**j** and Extended Data Fig. 3p). In **a**, **e**, and **f** decimals indicate the amounts of IP3R3 or BAP1 relative to α-tubulin, as per densitometry. In **d** and **h** decimals indicate the amounts of cleaved caspase-3 relative to α-tubulin, as per densitometry. For western blot source images, see Supplementary Fig. 2. For source data in **b**, **c**, **f**, **g**, **j**, see Supplementary Tables 1 and 2.

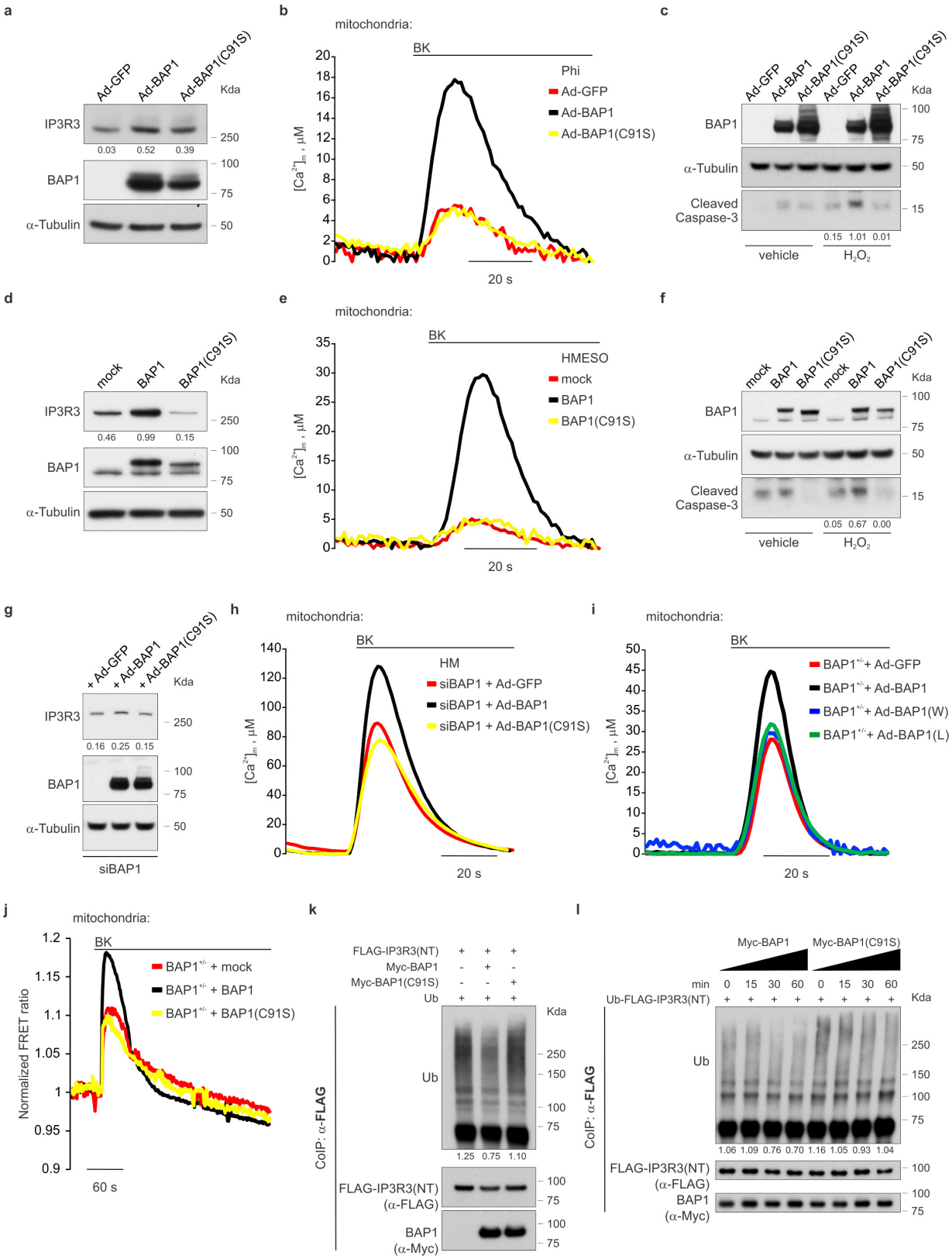

Extended Data Figure 8 | See next page for caption.

Extended Data Figure 8 | Effects of BAP1 rescue on IP3R3 protein levels, mitochondrial Ca^{2+} uptake, apoptosis, and IP3R3 deubiquitylation. a–**c**, Phi (human malignant mesothelioma cell line with mutated BAP1, see Extended Data Fig. 5d) cells were transiently transduced with wild-type BAP1 (Ad-BAP1), catalytically inactive BAP1(C91S) mutant, or control (Ad-GFP). Wild-type BAP1 stabilizes IP3R3 (**a**), increases $[Ca^{2+}]_m$ after stimulation with 1 μM bradykinin (**b**), and enhances apoptosis (**c**), while the catalytically inactive BAP1(C91S) mutant was less effective. In **c**, cells were treated with 500 μM H_2O_2 for 6 h and total cell lysates were prepared and analysed by western blot to compare cleaved caspase-3 levels. **d**–**f**, Stable clones of HMESO (see Extended Data Fig. 5d), in which we reintroduced wild-type BAP1, the catalytically inactive BAP1(C91S), or an empty vector (mock), showed that wild-type BAP1—but not the catalytically inactive BAP1(C91S) mutant—stabilizes IP3R3 (**d**), and increases $[Ca^{2+}]_m$ after stimulation with 1 μM bradykinin (**e**), and enhances apoptosis in cells treated with 100 μM H_2O_2 for 3 h (**f**). Total cell lysates were analysed by western blot to compare cleaved caspase-3 levels. **g**, **h**, Human mesothelial cells containing wild-type BAP1 were first silenced for BAP1 using siRNA and subsequently transduced with wild-type BAP1 (Ad-BAP1), catalytically inactive BAP1(C91S) mutant, or control (Ad-GFP). Wild-type BAP1 but not the catalytically inactive BAP1(C91S) mutant, (**g**) stabilizes IP3R3 and (**h**) increases $[Ca^{2+}]_m$ after stimulation with 1 μM bradykinin. **a**, **c**, **d**, **f**, **g**, Decimals indicate the amounts of IP3R3 or cleaved caspase-3 relative to α-tubulin, as per densitometry. **i**, *BAP1*$^{+/-}$ fibroblasts were transduced with wild-type BAP1 (Ad-BAP1), truncated BAP1(W) and BAP1(L), or control (Ad-GFP), and $[Ca^{2+}]_m$ was measured after stimulation with 1 μM bradykinin. **j**, Representative traces of single-cell Ca^{2+} measurements in *BAP1*$^{+/-}$ fibroblasts co-transfected with mitochondrial-targeted 4mtD3cpv and either BAP1 or the catalytically inactive BAP1(C91S) mutant; mock, co-transfection with an empty vector. Mitochondrial Ca^{2+} uptake was followed over time after stimulation with 1 μM bradykinin. **k**, Ubiquitylation assay showing that wild-type BAP1 (Myc–BAP1), but not BAP1(C91S) mutant, deubiquitylates the N terminus of IP3R3. HEK293 cells were co-transfected with Flag–IP3R3(NT) and either Myc–BAP1, Myc–BAP1(C91S), or empty vector. Ub, Ubiquitin. **l**, Ubiquitylation/deubiquitylation assay to monitor BAP1 deubiquitylation of Flag–IP3R3(NT). Either immunopurified wild-type Myc–BAP1 or catalytically inactive Myc–BAP1(C91S) were incubated *in vitro* with ubiquitylated Flag–IP3R3(NT). Protein levels were analysed by western blot with the indicated antibodies. The ladder of bands with a relative molecular mass of ≥90 kDa corresponds to ubiquitylated Flag–IP3R3(NT). Decimals indicate the amounts of ubiquitylated Flag–IP3R3(NT) normalized on total co-immunoprecipitated Flag–IP3R3(NT) at 90 kDa. For western blot source images, see Supplementary Fig. 2. For source data in **b**, **e**, **h**–**j**, see Supplementary Tables 1 and 2.

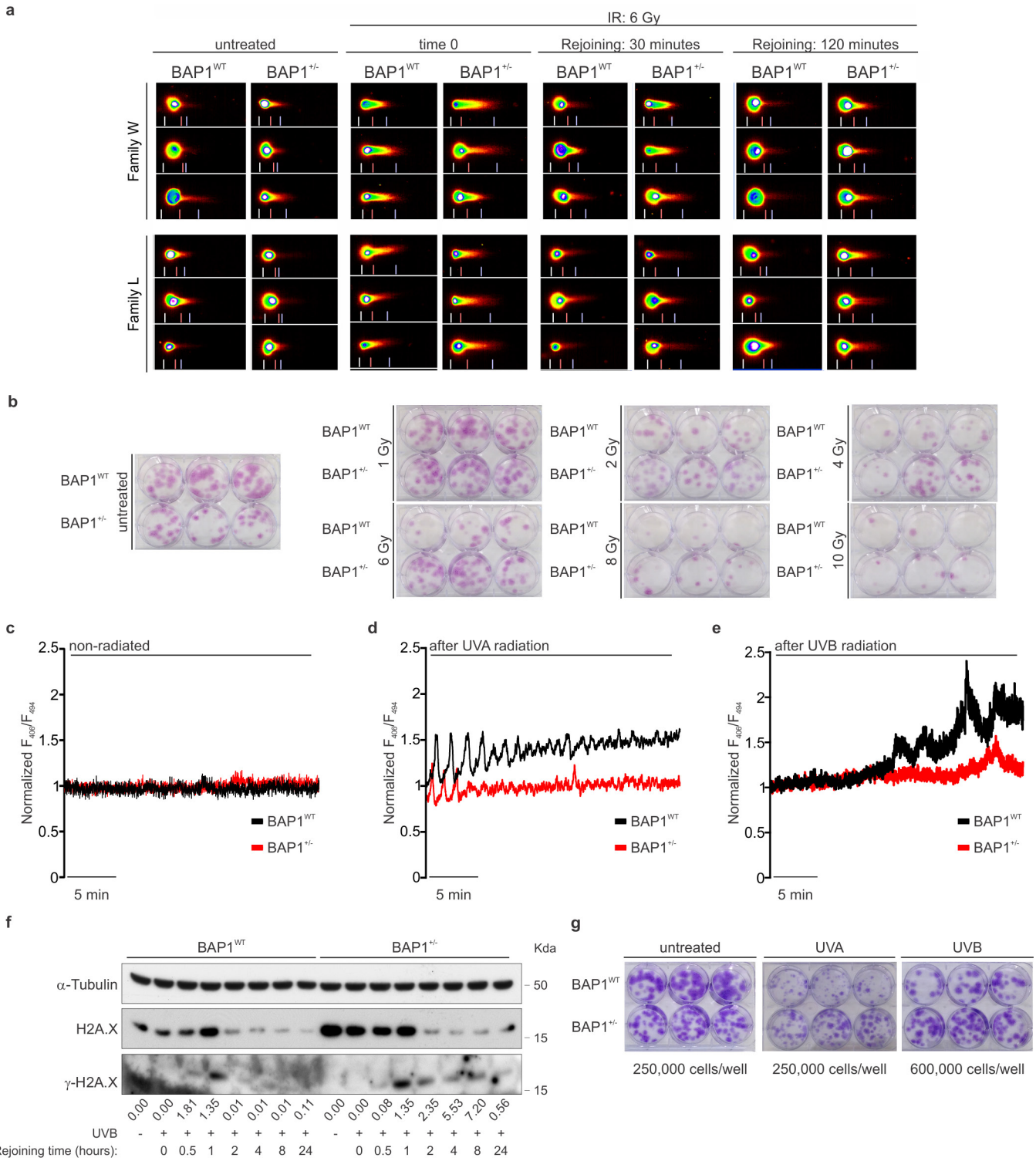

Extended Data Figure 9 | See next page for caption.

Extended Data Figure 9 | *BAP1*$^{+/-}$ fibroblasts exposed to ionizing or ultraviolet radiation show increased survival despite increased DNA damage. a, Representative images of comet assays. W and L family-derived fibroblasts were irradiated and analysed at the indicated time points (see also Fig. 4a). Representative results showing the rejoining of the DNA damage measured as the percentage of the tail moment at the indicated time points, after *BAP1*$^{+/-}$ fibroblasts and matched controls were irradiated with 6 Gy ionizing radiation. The length of the tail of the comet is proportional to the DNA damage. Note the increased tail length in *BAP1*$^{+/-}$ cells. **b**, Clonogenic assay showing a higher number of colonies in *BAP1*$^{+/-}$ fibroblasts after irradiation at the indicated amounts (see Fig. 4c). **c**–**e**, Reduced intracellular Ca^{2+} levels in *BAP1*$^{+/-}$ fibroblasts after ultraviolet radiation with UVA (340 nm) or UVB (312 nm). Dynamic measurements of cytosolic Ca^{2+} response were performed using the fluorescent Ca^{2+} indicator Fura-RED. **c**, Control; no changes in dynamic intracellular Ca^{2+} levels were detected over time in non-irradiated *BAP1*$^{+/-}$ fibroblasts and matched controls. **d**, **e**, Dynamic measurements of intracellular Ca^{2+} levels in *BAP1*$^{+/-}$ fibroblasts and matched controls after UVA (**d**) or UVB (**e**). Changes in intracellular Ca^{2+} responses over time are displayed as the ratio of fluorescence at 406/494 nm. Descriptive statistics are shown in Supplementary Table 1. **f**, Delayed DNA repair after UVB radiation in *BAP1*$^{+/-}$ fibroblasts. γ-H2A.X kinetics: *BAP1*^{WT} and *BAP1*$^{+/-}$ fibroblasts were exposed to UVB, and γ-H2A.X amounts were measured in cell lysates collected at the indicated time points. Total levels of H2A.X are shown as control. Densitometry: decimals indicate the amounts of γ-H2A.X relative to H2A.X. **g**, Clonogenic assay at 2 weeks after ultraviolet radiation: higher numbers of colonies in *BAP1*$^{+/-}$ fibroblasts after UVA or UVB exposure. Plating: untreated, 250,000 cells per well; UVA treated, 250,000 per well; UVB treated, 600,000 per well to accommodate for the higher potency of UVB that caused extensive cell death. Cells were exposed to 25 mJ cm^{-2}; see also Fig. 4d, e. Higher doses of 50, 75, and 100 mJ cm^{-2} killed all the cells within 2 weeks from exposure. For western blot source images, see Supplementary Fig. 2.

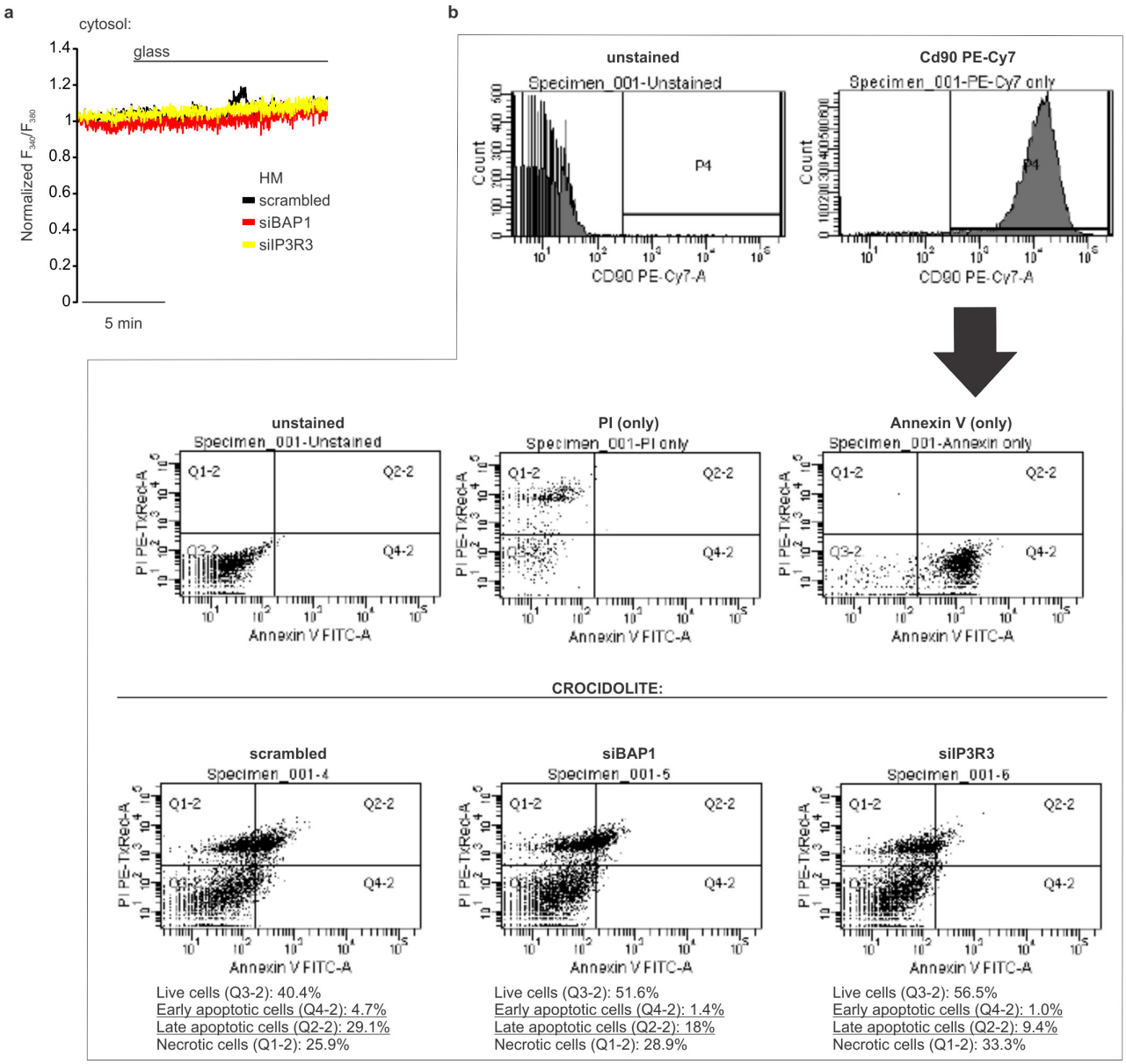

Extended Data Figure 10 | See next page for caption.

Extended Data Figure 10 | Human mesothelial cells and macrophages with reduced levels of BAP1 or IP3R3 are resistant to asbestos-induced apoptosis. a, Primary human mesothelial cells transfected with either scrambled siRNA, siBAP1, or siIP3R3, and exposed to glass, displayed no changes in intracellular Ca^{2+} concentrations (control for Fig. 4f). **b**, Flow cytometric analyses of human mesothelial cells silenced for BAP1, IP3R3, or scrambled control, and exposed to crocidolite asbestos for 24 h. Note that human mesothelial cells silenced for BAP1 or IP3R3 show a reduction in the percentage of apoptotic cells compared with scrambled control. **c**, **d**, BAP1 silencing in human THP-1 cells differentiated into macrophages leads to decreased IP3R3 protein levels (**c**), reduced mitochondrial Ca^{2+} uptake after stimulation with 100 μM ATP (**d**), and protection from apoptosis after treatment with 5 μg cm^{-2} crocidolite asbestos (**e**). In **d**, THP-1 cells were treated with 20 μM TPA for 24 h to induce monocyte differentiation into macrophages; subsequently, cells were transduced with WT mitochondrial-targeted aequorin (mtAEQ) for 24 h in the presence of TPA, and then transfected with control scrambled siRNA or siRNAs–BAP1 (siBAP1#1 and siBAP1#5) for an additional 24 h before Ca^{2+} measurements. In **e**, cells were treated with 20 μM TPA for 48 h, transfected with control scrambled siRNA, siBAP1#1, and siBAP1#5 for 24 h, and treated with 5 μg cm^{-2} crocidolite asbestos for an additional 24 h; total cell lysates were analysed by western blot to compare cleaved caspase-3 levels. In **c** and **e**, decimals indicate densitometrically determined IP3R3 or cleaved caspase-3 levels normalized to α-tubulin. For western blot source images, see Supplementary Fig. 2. **a**, **d**, For source data, see Supplementary Tables 1 and 2.